NMR and smFRET insights into fast protein motions and their relation to function

Paul Schanda[1] and Gilad Haran[2]

[1]Institute of Science and Technology Austria (ISTA), Am Campus 1, 3400 Klosterneuburg, Austria; email: paul.schanda@ista.ac.at
[2]Department of Chemical and Biological Physics, Weizmann Institute of Science, Rehovot 761001, Israel; gilad.haran@weizmann.ac.il

When citing this paper, please use the following: Schanda, P., Haran, G. 2024. NMR and smFRET insights into fast protein motions and their relation to function. Annu. Rev. Biophys. 53: Submitted. DOI: 10.1146/annurev-biophys-070323-022428.

Annu. Rev. Biophys. YYYY. AA:1–31

Keywords

molecular machines, allostery, single-molecule spectroscopy, spin relaxation, relaxation dispersion NMR

Abstract

Proteins often undergo large-scale conformational transitions, in which secondary and tertiary structure elements (loops, helices and domains) change their structures or their positions with respect to each other. Simple considerations suggest that such dynamics should be relatively fast, while the functional cycles of many proteins are often relatively slow. Sophisticated experimental methods are starting to tackle this dichotomy and shed light on the contribution of large-scale conformational dynamics to protein function. In this review we focus on the contribution of single-molecule FRET and NMR spectroscopies to the study of conformational dynamics. We describe briefly the state-of-the-art in each of each of these techniques and then point to their similarities and differences, as well as to the relative strengths and weaknesses of each. Several case studies in which the connection between fast conformational dynamics and slower function has been demonstrated are then introduced and discussed. These examples include both enzymes and large protein machines, some of which have been studied by both NMR and fluorescence spectroscopies.

Contents

1. INTRODUCTION

Proteins are dynamic molecules that possess a rugged, complex free-energy landscape and fluctuate between multiple conformational states (1, 2). The relative population of different states depends on environmental conditions such as pH, salt concentration and, most importantly, interaction with other molecules (ligands) (3, 4, 5). The motion between these conformational states involves crossing free-energy barriers with a broad range of heights, translating into a spectrum of time scales (2, 6, 7, 8, 9).

For nanoscale objects within a liquid, inertial forces are much weaker than viscous forces (10). Therefore, the rate of motion of a protein structural element can be shown to depend only on the shape of the potential energy surface for the motion and the viscous drag it incurs. Such considerations lead to a simple model for the motion of a large structural element within a protein, such as a domain, showing that it should take place on a time scale of nanoseconds (9, 11). This very fast motion can be slowed down if the relevant potential energy surface involves free-energy barriers, separating different conformations. The origin of such free-energy barriers is related to intramolecular interactions, including salt bridges, π-stacking interactions and hydrogen bonds, which need to be broken for the conformational change to occur (12). Remarkably, and in contrast to the fast nature of large-scale conformational transitions, productive biological processes such as enzyme catalysis or functional cycles of molecular machines are often relatively slow and sometimes even take many seconds (see as examples (13, 14, 15)), though there are cases where turnover is extremely fast, as happens, e.g., with the enzyme carbonic anhydrase (16). Understanding the molecular mechanisms of protein function requires understanding how these diverse time scales can be reconciled with each other. What are the rate-determining factors for the overall biological function? How important are fast motions for (slower) turnover? With a number of examples, this review will illustrate the significance of protein dynamics for biological processes.

For the sake of illustrating the relevant concepts, Fig. 1 depicts very schematically some possible conformational dynamics and simplified free-energy landscapes for an enzyme (A, B) and a directional machine (C). In the case of the enzyme, we consider two conformational states, an inactive state, in which the catalytic site is not formed for the chemical reaction

(left) and an active state that is arranged for allowing the reaction to proceed. We assume that substrate binding occurs (rapidly) within the inactive state.

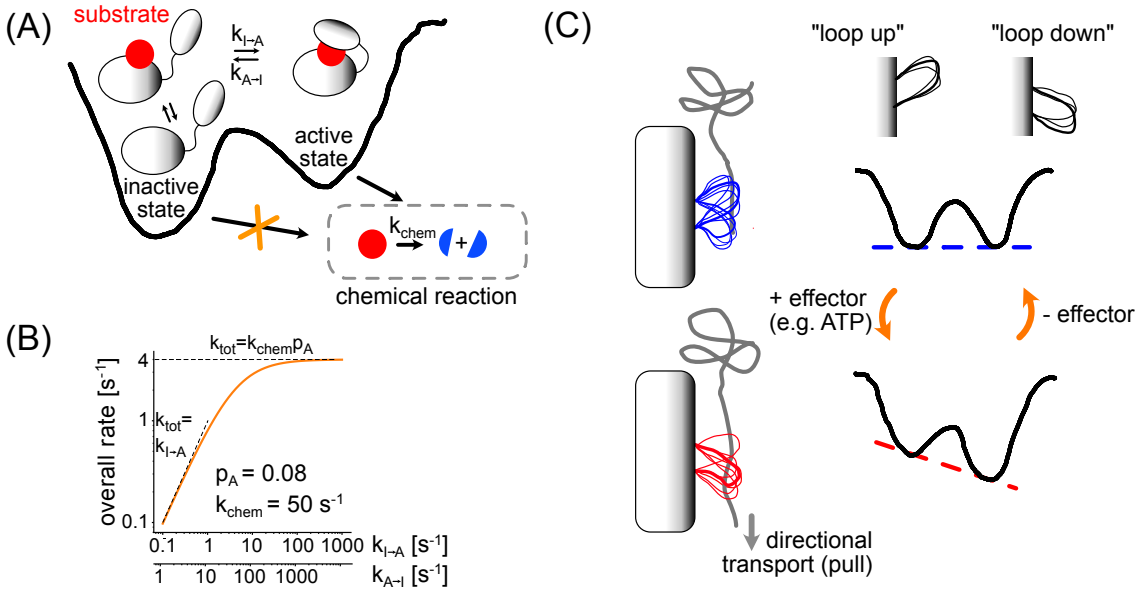

Figure 1: Schematic illustration of two functional processes in proteins involving exchanging conformational states. (A) An enzyme that interconverts between two conformations, while its chemical reaction takes place only from one of them. When the free-energy barrier between the two conformations is small, the chemical reaction is slower than the conformational transition; its kinetics then depends on the population of the active species. As the free-energy barrier is increased, the kinetics of interconversion between the two states may become important for the reaction. (B) Illustrative calculations of the total reaction rate of a turnover process for the scheme depicted in (A), assuming exchange between a state ("active", "A") that is able to transform a substrate with population p_A, and a state that is inactive for catalysis ("I"). The model, inspired by the HisHF study (Fig. 6), assumes that substrate binding is fast within the inactive-state ensemble. The overall turnover rate constant is modeled as $k_{tot} = k_{I\to A}k_{chem}/(k_{A\to I} + k_{I\to A} + k_{chem})$. The derivation and validity range ($k_{A\to I} \gg k_{I\to A}$ and/or $k_{A\to I} \gg k_{chem}$) have been reported in ref. (17) (Eq. 9); in the presented calculation $k_{A\to I} > 10k_{I\to A}$; $k_{chem} = 50$ s^{-1}. When the conformational exchange rates are small compared to k_{chem}, $k_{tot} = k_{I\to A}$, and when the exchange rates are large, $k_{tot} = p_A k_{chem}$. Dashed lines indicate these regimes. (C) A Brownian motor that translocates a polypeptide unidirectionally by alternating between two free-energy surfaces. On one free-energy surface, the populations of the two states of the depicted loop element might be equal. The second surface is skewed, leading to an imbalance between the two states. The different populations of the states, and the cycling between these energy landscapes lead to directional transport of the translocated polypeptide.

How is the turnover rate of the enzyme linked to the conformational dynamics? On one side of the spectrum of possibilities, conformational dynamics could be slower than

the intrisic "chemical" step. In this case, every time the active state forms, the chemical turnover would occur. Thus, the kinetics of enzymatic turnover would be determined by the *kinetics* of the dynamic process. Calculations of the overall turnover rate constant (k_{tot}) as a function of the rate of formation of the active state ($k_{I\rightarrow A}$; keeping the active-state population constant; Fig. 1B) show that in this regime $k_{tot} = k_{I\rightarrow A}$.

On the other end of the spectrum of possibilities, motion is (much) faster than the turnover, as might be expected based on the fundamental considerations discussed above. Schematically, in this scenario, fast exchange would be present between an inactive and an active state, and the latter can – but rarely does – lead to turnover. The conformers rapidly equilibrate between consecutive turnover events. Therefore, the kinetics of turnover in this case depends on the *population* of the conformation that allows turnover, rather than the rate of exchange. In this case, it is the equilibrium level of active state that determines the overall process, i.e. $k_{tot} = p_A k_{chem}$ (Fig. 1B; dashed horizontal line).

The same reasoning can apply to a machine that allows for unidirectional mechanical translation (Fig. 1C). Here we schematically depict an exchange between two states, in which a loop has different orientations, and binds to a peptide chain. These two loop orientations may have similar free energies, and the loop visits the two conformations through thermal motion; a trigger such as ATP binding or hydrolysis can switch the free-energy landscape to one on which these two states become populated to a different extent (lower part of this Fig. 1B). By alternating between these two energy landscapes, the protein can transport the peptide unidirectionally, e.g., through a tunnel, as in the case of AAA+ proteins. This is an example of a Brownian motor, with energy pumping leading to an exchange between two (or more) free-energy surfaces on which diffusive motion takes place (18). Brownian motors are also characterized by rapid equilibration that occurs each time they switch between free-energy surfaces, as in the enzyme case. However, this switching also leads here to mechanical motion.

In both scenarios, dynamics are crucial for function. Yet, the overall rate constant of turnover can be governed by either the kinetics of motion or by the thermodynamics of the exchanging states. Understanding how proteins achieve their function, thus, requires knowledge of the kinetics, thermodynamics (populations) and structural details of the motions, in relation to the overall function.

Multiple methods for the experimental characterisation of protein dynamics are available, including steady-state and time-resolved fluorescence spectroscopy (19, 20), x-ray and neutron scattering techniques (21, 22), time-resolved x-ray diffraction (23, 24), high-speed atomic-force microscopy (25), electron paramagnetic resonance spectroscopy (26, 27) and more. Nuclear magnetic resonance (NMR) spectroscopy (28, 29, 30) and single-molecule Förster resonance energy transfer (smFRET) (31) spectroscopy currently stand out as particularly powerful techniques to study conformational dynamics of proteins and will therefore be in our focus in this review.

We will start by providing the reader with a basic understanding of the strengths, challenges and complementarities of smFRET and NMR experiments in tackling such dynamics (section 2). We will then illustrate the link between protein dynamics and turnover using specific cases (section 3), and demonstrate how the measured motions play an important role in the activity of the described proteins.

2. SmFRET and NMR spectroscopies provide insights into dynamics

Both smFRET and NMR are spectroscopic techniques, i.e. they gain insights into molecules by the interaction of spectroscopic probes (electronic transition dipoles within dyes and spins within atoms, respectively) with electromagenetic irradiation. Fig. 2A schematically sketches motions of a protein, which alter the environments of and distances between such spectroscopic probes. NMR and smFRET gain insight into these motions via the effect that dynamics have on spectroscopic signals. Here we briefly review the underlying principles, and the approaches that allow shedding light onto structural dynamics. These considerations then lead us to highlighting how the two methods can complement each other.

2.1. FRET insights into protein dynamics at the single-molecule level

FRET is a phenomenon that stems from the interaction between the transition dipoles of two quantum emitters as they get close together (32). Excitation of one emitter, termed the "donor", leads to migration (or transfer) of the energy to the second emitter, the "acceptor", when the emission spectrum of the first and absorption spectrum of the second overlap. The strong sixth-order distance dependence of the FRET efficiency has made this phenomenon a valuable "spectroscopic ruler" for biological samples (33). The useful distance for the ruler depends on the pairs of fluorescent dyes used, but usually spans the 2-10 nm range (Fig. 2B). Importantly, the dipolar interaction between the emitters also depends on their mutual orientation (34). However, in solution this mutual orientation is often averaged by rotational diffusion of the dyes within the molecule, allowing a relatively straighforward estimation of the so-called "Förster distance", R_0, which is required for the calculation of the FRET efficiency: $E = 1/(1+(R/R_0)^6)$, where R is the distance between the fluorophores (34).

For many years, FRET experiments have been conducted in bulk solutions, including sophisticated applications to determine the distribution of distances within biomolecules (35). Such studies have provided important insights on biomolecular structure and interactions, but have often suffered from issues such as partially labeled samples and background signals. Single-molecule FRET (smFRET) spectroscopy has emerged in recent years as a powerful method to gauge distances within biomolecules, and has been shown to overcome many difficulties of bulk FRET studies (36, 37).

SmFRET is particularly suitable to observe distance changes due to conformational transitions within a biomolecule and provide information on the time dependence of these transitions. In order to conduct smFRET experiments to study protein dynamics, a protein of choice is first labeled with two fluorescent dyes. Typical FRET dyes are conjugated multi-ring aromatic molecules; they are often attached to cysteine residues via one of several covalent chemistries, though other residues, such as unnatural amino acids, have also been used (38). The labeling positions are selected based on several considerations, including the need to sample a particular conformational transition of the protein, the exposure of the two sites to the solution to facilitate attachment of the fluorescent dyes and enable free local rotation and a measured absence of any effect of labeling on the stability or activity of the protein.

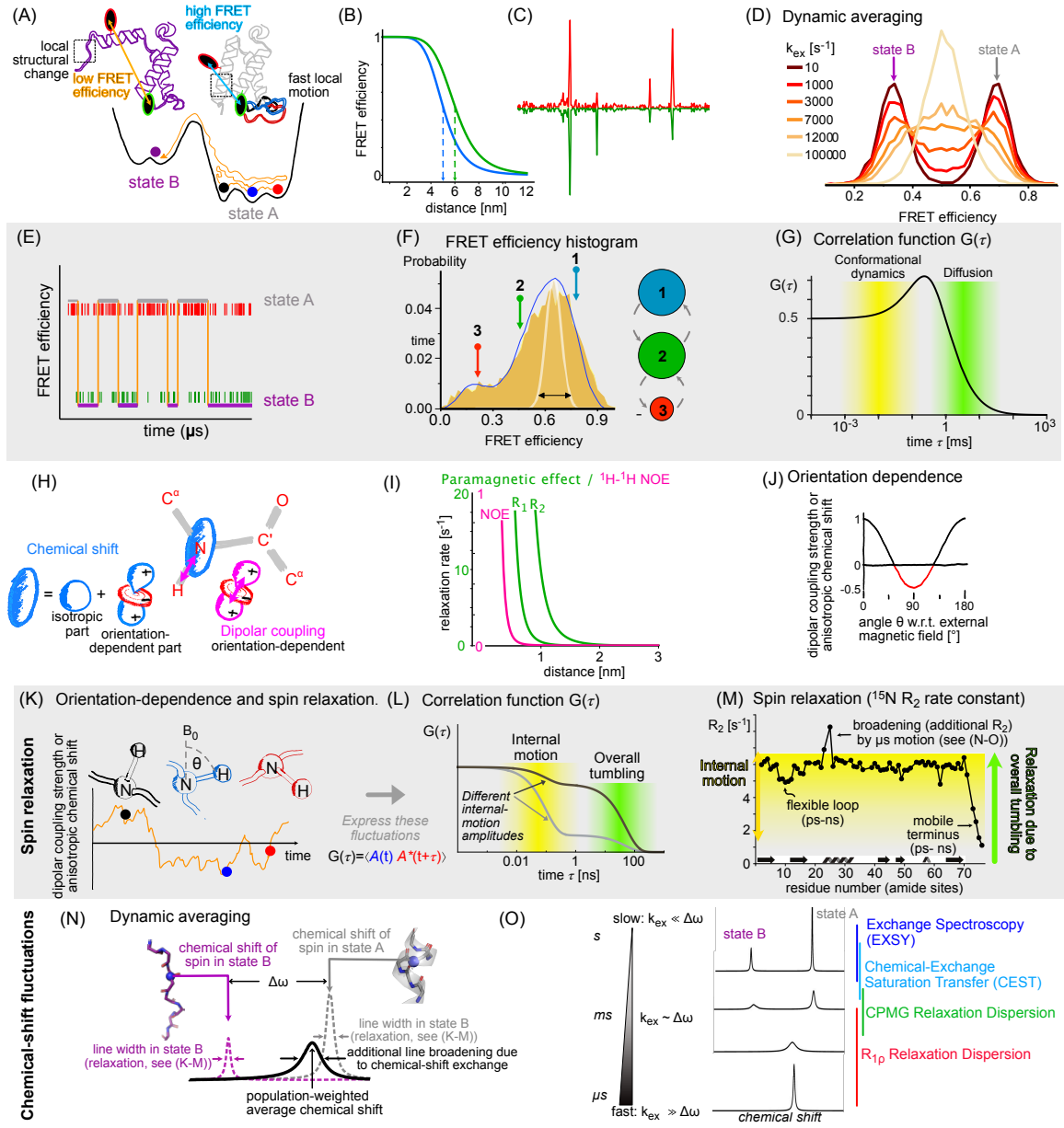

Figure 2

Figure 2: Continued: Complementary views on protein dynamics from smFRET (A)-(G) and NMR (H)-(O) spectroscopies. (A) Free-energy profile for a protein interconverting between two main conformations, states A and B. The dynamics of this interconversion can be probed via the fluctuation of the distance of smFRET labels, and the fluctuations of NMR interactions. (B) The accessible range for FRET measurements depends on molecular parameters of the dyes, as embodied by the Förster distance. The FRET efficiency dependence for two different Förster distances is shown in the figure. (C) A series of photon bursts, as measured in a single-molecule experiment on freely diffusing molecules. Green and red are emissions in the donor and acceptor channels, respectively. (D) A FRET efficiency histogram, calculated from multiple photon bursts, encodes conformational dynamics. Consider a transition between two conformations. When the interconversion rate is small, two clear peaks are seen in the histogram. As the interconversion rate increases, the histogram gradually collapses to a single peak. (E) Each photon burst is in fact a time series of photon arrival times, i.e., a photon trajectory. A momentary modulation of the relative numbers of photons in donor and acceptor channels can be due to transitions between conformational states. The dynamics are retrieved by statistical analysis performed at the level of photon trajectories. (F) A FRET efficiency histogram of a molecule with three conformational states. The white line and black arrow demonstrate the histogram width expected in the absence of conformational dynamics. The extra width is due to dynamics, and analysis retrieves the three states, whose positions are depicted with arrows on the histogram. The scheme on the right indicates the relative populations of the three states (circle areas), their FRET efficiency values, and interconversion rates. (G) Conformational dynamics can also be retrieved from fluorescence correlation functions. In particular, a donor-acceptor cross-correlation function shows a rising component on the timescale of the dynamics. At longer times, the correlation function decays due to the diffusion of the protein molecules through the laser beam. (H) A sketch of a peptide plane, highlighting interactions of the ^{15}N spin with its environment: the chemical-shift tensor (blue) is most often decomposed into its (non-zero) isotropic part and the chemical-shift anisotropy; the magenta symbol denotes the ^{1}H–^{15}N dipolar coupling, whose isotropic part is zero. Red denotes an interaction with negative sign. The instantaneous interaction strength is given by the projection of these tensors onto the direction of the external magnetic field. (I) Distance dependence of the ^{1}H–^{1}H NOE effect (pink) and paramagnetic relaxation rate constants of a ^{1}H spin as a function of its distance to a spin label (electronic correlation time 100 ns). (J) Orientation dependence of anisotropic interactions (CSA, dipolar coupling), $(3\cos^2\theta - 1)/2$; the angle θ is between the principal axis of the tensor and the static magnetic field. Note that there are more realisations of θ perpendicular to the magnetic field than parallel, and isotropic sampling of all θ averages the interaction to zero. (K) Dynamics modulate the orientation of the interaction strength. This fluctuation is expressed as correlation function (L). The efficiency of spin relaxation depends on the amplitude and time scale of this fluctuation. (M) An example of ^{15}N transverse relaxation rate constants (called R_2) as a function of the residue number in the protein ubiquitin in solution (BioMagResBank accession number 6470). Due to overall tumbling, relaxation is dominated by tumbling; differences point to local motion. As R_2 also senses chemical-shift line broadening, several residues have enhanced R_2. (N) Schematic depiction of chemical-shift based line broadening. (O) Different exchange rate constant result in different appearance of the peak positions and line widths. Panels C and E were adapted from (37). Panel F was adapted from (39).

SmFRET experiments are often conducted on molecules immobilized on a surface, and the signals are probed using a sensitive fluorescence camera, which limits the time resolution to a few milliseconds (40). A higher time resolution can be achieved in an smFRET experiment conducted using confocal microscopy and detectors with single-photon sensitivity.

Such experiments are conducted on either immobilized molecules or molecules that move freely in a dilute solution (37). In the latter case, labeled protein molecules are allowed to diffuse through a focused laser beam, and their concentration is selected such that the probability to have more than one molecule in the beam at any moment of time is small; this typically entails a picomolar concentration. The laser excites the donor dye, and emitted light from both donor and acceptor dyes is collected using photon-counting avalanche photodiodes. In a more advanced version of the experiment, two lasers are used in a pulse-interleaved configuration, so that both donor and acceptor are intermittently excited (41). This allows monitoring and filtering out molecules or data segments in which the acceptor dye is inactive.

A typical smFRET data set from freely diffusing molecules contains several thousand events of molecules passing through the laser beam and emitting light, which are termed 'photon bursts' (Fig. 2C). The simplest method to analyze such data involves calculating the FRET efficiency value of each burst and histogramming the set of values obtained in this manner. Observation of a FRET efficiency histogram (Fig. 2D) can already provide some precious information on conformational dynamics. For example, the histogram can explicitly show more than a single FRET efficiency peak, suggesting the existence of several distinct species in the sample. The question is then whether and how fast these species exchange. If the exchange is significantly slower than the typical diffusion time of a molecule through the laser beam, which is of the order of 1 ms, the FRET efficiency histogram will show clearly separated peaks. As the exchange between species becomes faster and faster, the separate peaks start to 'mix', eventually generating a histogram with a single peak when the exchange time is much shorter than 1 ms. This is equivalent to the familiar phenomenon of 'motional narrowing' in spectroscopy (see also in the NMR part below).

Various methods have been devised to qualitatively or semi-quantitatively analyze FRET efficiency histograms. For example, burst-variance analysis (42) bins each burst into bins with a fixed number of photons and calculates the variance of the FRET efficiency values in these bins. Comparison of this variance to the one given by shot-noise statistics provides a measure for the occurrence of fast dynamics in the data. Photon-distribution analysis methods take into account the shot-noise statistics together with a kinetic model in order to obtain the complex shape of a FRET histogram and thereby extract the model parameters that best fit the data (43).

In recent years, analysis methods that operate at the level of the photon trajectories, i.e. the time series of photon arrival times that underlie photon bursts (Fig. 2E), rather than on FRET efficiency histograms, have been introduced. These methods, which benefit from the current ability to measure accurately the arrival times of donor and acceptor photons on single-photon detectors, are typically variants of Hidden Markov Model (HMM) analysis, a popular machine-learning technique (44). They start by evaluating the likelihood to obtain a measured set of photon trajectories, given that the dynamics of the system can be described by a specific kinetic process involving several states. This likelihood is then maximized to extract populations and FRET efficiency values of the conformational states, as well as their interconversion rates (45, 46), as depicted schematically on the histogram of Fig. 2F.

Kinetic rates can also be measured by various forms of fluorescence correlation spectroscopy (FCS) (47). In FCS (Fig. 2G), the autocorrelation function of a single-color emission or the cross-correlation of the donor and acceptor emissions is calculated. Specifically, the time correlation of intensities is calculated as $G(\tau) = \langle(\delta I(t)\delta I(t+\tau))/\langle I(t)\rangle^2$,

where $\delta I(t) = I(t) - \langle I(t) \rangle$ is the deviation from the mean intensity. For a cross-correlation function, $I(t)$ and $I(t+\tau)$) refer to the intensities of the two different channels. While at long time scales (hundreds of microseconds to milliseconds) the correlation function reports on the translational diffusive motion of a labeled protein, at shorter times it reports on internal dynamics, including photophysical processes, such as triplet-state kinetics, and conformational dynamics. In particular, conformational changes lead to anti-correlated donor and acceptor emissions: when the distance changes from short to long, the donor emission increases, while the acceptor emission decreases (48). This anti-correlated behavior is manifested as a rising component in the donor-acceptor cross-correlation function on the time scale of the conformational dynamics (Fig. 2G). In intrinsically disordered proteins this time scale is very fast (49), but in folded proteins demonstrating transitions between different stable conformational states, the time scale of the rising component in the correlation function can be significantly longer, i.e. tens or even hundreds of microseconds. Correlation functions also play a role in NMR spin relaxation, where they refer to the time correlation function of spin interaction strengths, as explained below.

2.2. Nuclear magnetic resonance views of proteins at the atomic resolution

NMR is a phenomenon that stems from the interaction between the magnetic moment of an atomic nucleus and magnetic fields to which this nucleus is exposed (50). Many atoms in biomolecules possess such a property, called nuclear spin, a quantum-mechanical property. In biomolecules, particularly important NMR probes are ^{1}H and ^{31}P, present at ca. 100% natural abundance, and ^{13}C and ^{15}N, which have low natural abundance but can be easily enriched by producing proteins in isotope-labeled media. As the NMR-observable probes lie within the nucleus, they generally come without chemical modification of the molecule (with the exception of NMR experiments that exploit paramagnetic labels to probe interactions of nuclear spins with unpaired electrons, see below).

When placed in an intense static magnetic field generated by a superconducting magnet, the energy levels of a spin become non-degenerate. Compared to fluorescence spectroscopy, the energy difference in NMR is tiny. This has several consequences. First, the energy levels are populated almost equally, leading to very low sensitivity, as spectroscopic transitions rely on population differences. Second, spontaneous emission of photons is virtually absent, unlike in optical/fluorescence spectroscopies. Consequently, the detection principle in NMR is not based on measurement of emitted photons. Instead, NMR spectroscopy uses short intense pulses of an electromagnetic field in the radiofrequency range ("RF pulses") to excite the spin system and create a coherent superposition of the magnetic moments of the spins of many (typically $>10^{15}$) molecules. This bulk magnetic moment rotates (precesses) inside the intense magnetic field, which generates an electric current in a coil wound around the sample, termed a free-induction decay (FID). The frequency of this alternating current is directly proportional to the spins' energy level difference, the so-called Larmor frequency or resonance frequency. The precession lasts until the coherent superposition of the magnetic moments of the spins decays due to relaxation (see below), which is often many tens of milliseconds. In order to be able to determine the frequency precisely, the NMR signal has to be followed over many milliseconds. This fact, together with the need to repeat this excitation/observation several times to improve sensitivity, means that NMR can not easily observe motion in real time (unlike FRET). However, real-time NMR is useful in some contexts e.g. for measuring the signal of substrates while being turned over, i.e., the reaction

kinetics (such as in the case of DcpS discussed in section 3.4); moreover, off-equilibrium processes such as protein folding and hydrogen-deuterium exchange can be measured so long as they occur on a seconds-minutes time scale (51, 52); kinetics of protein modifications can even be monitored in the complex environment of intact cells (53, 54). A particularly exciting development is the study of off-equilibrium kinetics by using either light pulses or a fast pressure jump to generate an off-equilibrium situation, and follow the evolution of the protein with millisecond time resolution (55). In the remainder of this article, however, we focus on equilibrium dynamics measurements.

The reason why nuclear spins can report on structural fluctuations is because the instantaneous resonance frequency of a spin depends on its environment, which creates local magnetic fields via two effects (Fig. 2H):

(i) the electronic environment of the spin, which is exquisitely sensitive to the chemical nature and local conformation; the quantity describing this effect is called chemical shift, and is described by a rank-2 tensor. It is often decomposed into an orientation-dependent part also called chemical-shift anisotropy (CSA) and its average value, also called isotropic chemical shift, and

(ii) the interaction of the magnetic moments of two spins, also called dipolar coupling. This coupling has an analogy to the coupling of dipole moments of fluorescent dyes engaged in FRET, but the interaction is weaker and therefore the distance range over which it acts is much shorter. The dipolar coupling between two nuclear spins barely has detectable effects beyond 1 nm. If one of the spins is an unpaired electron, the range is somewhat larger, and effects up to 2.5 nm can be sensed (Fig. 2I). An unpaired electron can be found in proteins with certain metal sites, or added by covalently binding stable radical tags, also denoted as paramagnetic labelling.

Motions lead to a time-dependent fluctuation of these interactions, and the consequences of these fluctuations allow NMR to report on dynamics, either via spin relaxation experiments or due to the fact that the observable quantities are averages; the magnitude of the averaged quantity, compared to a "rigid-limit" magnitude, reports on the motional amplitude, and also the precise way the averaging manifests contains information. These two types of experiments are described in the following.

Spin relaxation is the process by which the ensemble of nuclear spins, which have been moved away from their thermal equilibrium by RF pulses, returns to its equilibrium. In equilibrium, the spins of the ensemble of molecules are not in phase with each other (no "coherence") and their levels are populated according to Boltzmann statistics. Spins relax because of the local fluctuating magnetic field they are exposed to, and it fluctuates because dipolar couplings and chemical-shift anisotropies depend on the orientation within the magnetic field (Fig. 2J): the stochastic rotation of the whole molecule as well as internal motion render the magnetic field at the location of the nucleus time-dependent (Fig. 2K). If these fluctuations of the local magnetic fields occur at the right frequencies and are of large amplitude, they are efficient in inducing relaxation. Thus, the distribution of the frequencies of motions is relevant for the speed at which spins relax. This distribution is directly related (by Fourier transformation) to the correlation function that describes the time evolution of an interaction, e.g., the dipolar coupling (Fig. 2L). Therefore, by measuring relaxation rate constants, NMR spectroscopists gain access, although indirectly, to the correlation function describing the fluctuations of bonds, domains or an entire protein. Fig. 2M shows an example of a spin relaxation rate constant of backbone ^{15}N nuclei in a small protein, readily measurable in an NMR experiment in an atom-by-atom manner.

One can see that while the relaxation rate constants for many of the ^{15}N backbone amides are similar, reflecting the fact that the overall tumbling is common to the whole protein, there are important residue-to-residue differences. Experiments of this type reveal local flexibility. Such studies of internal motion are very insightful, e.g., for probing the entropy of ligand binding (56), motions of intrinsically disordered proteins (57), or how one domain moves relative to others (see the case of ClpB in this review below, Fig. 3B).

A limitation of NMR relaxation measurements in solution is that internal motion slower than the tumbling would not change the correlation function and therefore cannot be seen, since overall tumbling brings the correlation function to zero (Fig. 2L). This limitation is lifted if the molecules are immobilised: in a system that does not undergo fast overall tumbling (e.g., a crystal, a liposome-embedded protein or large protein assemblies) magic-angle spinning (MAS) NMR relaxation is the method of choice (58, 59). In this method, the sample is rapidly spun at an angle of 54.7° relative to the static magnetic field. This spinning averages orientation-dependent interactions to zero, which means that the broad spectral patterns that are due to CSA and dipolar interactions collapse into a single line, similarly to what the overall Brownian tumbling in solution achieves. However, as the stochastic overall tumbling is absent, MAS NMR senses internal motions over all time scales (ps-s), such as the motions of entire secondary structure elements within a membrane or the motions of entire domains within complexes or crystals (60, 61, 62, 63, 64).

Besides inducing spin relaxation, motion can also be seen in NMR experiments by measuring how the above-introduced NMR interactions are averaged. The most important observable in this respect is the isotropic chemical shift, which gets averaged due to dynamics. Figure 2N illustrates isotropic chemical-shift averaging with a simple example of a part of a molecule that exchanges between an unfolded state (purple) and a folded state (grey). Because the local environment (dihedral angles, etc) differs in the two states, the isotropic chemical shift of each atom differs. While collecting the NMR signal (FID), the molecule may change its state multiple times. The resulting spectrum depends on how frequently the molecule has exchanged, as well as how different the chemical shifts of the exchanging states ($\Delta\omega$, in units of Hz) are: in case the exchange is very slow ($k_{ex}=k_{forward}+k_{backward}\ll\Delta\omega$), the signals of the individual states are observed with peak heights reflecting their relative populations (Fig. 2O). For a very fast exchange ($k_{ex}\gg\Delta\omega$), a single peak at a population-weighted average position is observed. In the gradual transition between these two extremes, exchange is manifested as line broadening (Fig. 2O). This broadening can be understood as a loss of coherence among the ensemble of spins in the sample. Note the parallel to averaging in FRET histograms, Fig. 2D. The chemical-shift averaging can by itself already be very instructive. For example, when a symmetric homooligomeric complex binds a ligand, the symmetry is expected to be broken. If the complex is very dynamic, such that on average all subunits experience the same environment, the NMR spectrum would still show a single, time-averaged peak (65, 66).

Most importantly, the line broadening due to exchange processes can be quantified, and it can be modulated by RF pulses, and such approaches are extremely powerful to obtain insights into the thermodynamics (populations of state), kinetics (exchange rates) and structural aspects of the exchanging states. Various techniques have been developed to probe conformational exchange in different regimes (reviewed, e.g., in (28)).

(i) When the exchange is slow (tens to hundreds of ms), and the populations of the exchanging states are sufficiently large such that NMR signals of the individual states are observable, longitudinal magnetization-exchange spectroscopy (EXSY) experiments are

useful. EXSY two-dimenstional spectra report which NMR signal (state) "exchanges" with which other NMR signal and allow to retrieve the populations and kinetics of exchange.

(ii) If the population of one of the states is too small to observe the signals corresponding to it, then EXSY generally fails; however, the presence of the minor state can be revealed by so-called chemical-exchange saturation transfer (CEST) experiments. Minor states populated to 0.5% or more can be studied in detail (67) so long as the exchange occurs on time scales from several ms to tens of ms.

(iii) Faster exchange processes can be studied by relaxation-dispersion (RD) NMR techniques. In this class of experiments, the line width, or more precisely the lifetime of the coherent superposition of spins, is measured in the presence of RF irradiation, either using a train of recoupling pulses (Carr-Purcell-Meiboom-Gill, CPMG RD) or continuous irradiation ($R_{1\rho}$ RD). By changing the frequency at which these pulses are applied (CPMG RD) or the power of the applied field ($R_{1\rho}$ RD), the effects of exchange on the signal decay can be altered. Accordingly, by systematically exploring the dependence of coherence decay on these pulse-sequence parameters, one can obtain quantitative information about the populations of the exchanging states, the kinetics of exchange and the chemical-shift difference.

An exciting possibility is the determination of near-atomistic 3D structures of these short-lived, conformationally "excited" states, which are not even visible directly in NMR spectra. The way to determine structures is through the chemical shifts of the excited state, which can be determined by CPMG or CEST experiments. Combining many types of excited-state chemical shifts (^{15}N, $^{1}H^{N}$, ^{1}Hα, ^{13}Cα and ^{13}C'), the structures of short-lived intermediates of binding or folding have been determined (68, 69).

In addition to the averaging of isotropic chemical shifts, also dipolar couplings and CSAs are averaged. In solution, where all orientations are sampled isotropically, the time average is zero, and therefore one does not learn about dynamics from measuring this time-averaged value. In MAS NMR, however, where overall tumbling is absent, the averaged dipolar couplings and CSAs report on the amplitude of location motion. In this case, measuring the dipolar coupling or CSA, and comparing the obtained values to those expected for the case of a rigid molecule, allows to directly obtain the amplitude of motion; this value, generally expressed as an order parameter (ranging from 1 for no motion to 0 for full isotropic motion) reports on motion faster than tens of µs. A case where the dipolar order parameter has been used is presented in Fig. 5B.

Lastly, 3D structures determined by NMR from the nuclear Overhauser effect (NOE; a dipolar-coupling based relaxation effect) also comprise information about the structural heterogeneity, and thus about dynamics. In this context, the recent development of "exact NOE" approaches is particularly worth mentioning (70, 71, 72, 73, 74). By measuring the buildup of the NOE effect and taking care of possible relayed transfer of magnetisation, structures can be determined at higher precision. Particularly, a set of experimentally determined atom-atom distances (typically several thousands) may not be in agreement with a *single* structure; thus, two or more conformations may need to be invoked to explain the experimental data. These structures represent the co-existing conformations present on time scales up to milliseconds. The fact that distinct sets of structures are determined also allows for the detection of correlated motions, e.g., of a set of side chains. While this technique is not yet widespread, very promising applications have been reported (75, 73).

2.3. NMR and smFRET ideally complement each other

SmFRET and NMR spectroscopies have several formal similarities, many practical differences and many complementarities, some of which we discuss here.

(i) An obvious difference between the two methods is in their sensitivity, which stems from the very different types of spectroscopic transitions used in the two (electronic and nuclear, respectively), and very different energy-level splittings. In addition, fluorescence spectroscopy in general is a background-free method, as it relies on photon emission. Therefore, FRET can be studied using solutions with picomolar concentrations and even on the single-molecule level. NMR, on the other hand, has to rely on large ensembles of molecules and concentrations of many micromolars (solution) or quantities of ca 0.5 mg or more (solids). This is generally an advantage of smFRET, although when studying complexes with low or medium affinity, the low concentrations may entail specialized techniques (e.g. (76)).

(ii) NMR experiments simultaneously probe the dynamics of multiple, often hundreds of individual sites within a protein, each reporting on its local environment (<8-10 Å). Information about collective processes, e.g. rearrangement of a whole secondary structure element or domain unfolding, can be deduced from the fact that multiple probes in that structural element report on the process. SmFRET spectroscopy usually probes a single donor-acceptor pair at a time, though studies with three fluorescent dyes and even four have been reported. Experiments on multiple donor-acceptor pairs can be performed (77), but they require separate preparations. FRET experiments probe primarily the inter-probe distance fluctuations, though accompanying fluorescence anisotropy studies can also probe local motion of each of the dyes.

(iii) Most smFRET experiments probe dynamic processes as real-time fluctuations of the FRET signal around equilibrium. NMR experiments probe dynamics indirectly via the effects of relaxation, exchange broadening or cross-peaks between signals of distinct states. NMR detects the ensemble of molecules, rather than probing individual molecules fluctuating at equilibrium.

(iv) The FRET signal is directly linked to a distance; hence a change in the FRET signal is naturally mapped onto a change in intramolecular distance and related to a particular conformational change. NMR experiments probe local changes. The latter can be very informative on even subtle rearrangements, local unfolding or ligand binding, which might be difficult to capture by smFRET because of the short length scales at which they take place. NMR spectroscopy does not provide directly a "ruler" of what the conformational change is, but one may understand the structural changes occurring, using the chemical shift or distance-dependent parameters (NOEs or paramagnetic effects). These properties are highly complementary: one may combine the short-range (NMR; up to ca. 0.8 nm with NOEs and 2 nm with PRE effects) and long-range (FRET; 2 - 10 nm) views of biomolecular motions. NMR may see processes of small amplitude (e.g. loop motions) which are too small to be seen by smFRET.

(v) The observable probes required for NMR do not alter the protein at all. FRET labels are bulky organic dyes, and one needs to evaluate any possible perturbation induced by their presence.

(vi) Finally, in general in kinetic experiments one extracts combinations of forward and backward rate constants. In order to calculate the separate rates, one needs to know or compute also the relevant equilibrium constants. For example, in NMR relaxation-dispersion experiments, one needs to fit populations and exchange rates from the RD profile,

and when the exchange becomes fast (μs range) populations may be difficult to retrieve (78). In contrast, a peculiar strength of single-molecule experiments in general, and smFRET experiments in particular, is that the separate forward/backward rates can be directly obtained from the data. This is particularly useful under instances where it might not be clear that the studied system is at equilibrium.

These different sensitivities of the two techniques suggest that their combination allows exceeding the information that each individual method could provide. Indeed, combined studies are gaining momentum. For example, in studies of intrinsically disordered proteins and their complexes, one gains insight into local backbone conformations and dynamics from NMR, while the overall dimensions of the polymer can be retrieved from smFRET (79, 49). Studies of this kind have been reviewed (80).

Below we discuss several cases where NMR and smFRET (or both) have been used to investigate molecular motions and their link to protein function. Rather than attempting an exhaustive coverage of published studies, we focus on cases where fast motions have proven to be crucial for slower functional processes.

3. Motions in molecular machines and their link to function

3.1. Domain motions in a disaggregation machine

ATPases associated with various cellular activities (AAA+) are hexameric, ring-shaped proteins that translocate substrates through their central pore (81, 82). Their structural and functional complexity involves multiple internal allosteric pathways and related conformational dynamics. We focus here on the conformational transitions of ClpB of bacteria and p97/VCP of eukaryotic cells, both functional in remodeling substrate proteins (83, 84). ClpB is an ATP-dependent molecular chaperone operating as a protein disaggregation machine (83), while p97/VCP participates in multiple cellular functions, including DNA replication, transport processes, immune signaling, and protein degradation (84). Interestingly, the protomers of both proteins are composed of an N-terminal domain (NTD) and two nucleotide binding domains, which in the case of ClpB are termed NBD1 and NBD2. ClpB also contains a regulatory middle domain (M-domain), which is a coiled-coil structure connected to NBD1 (Fig. 3A).

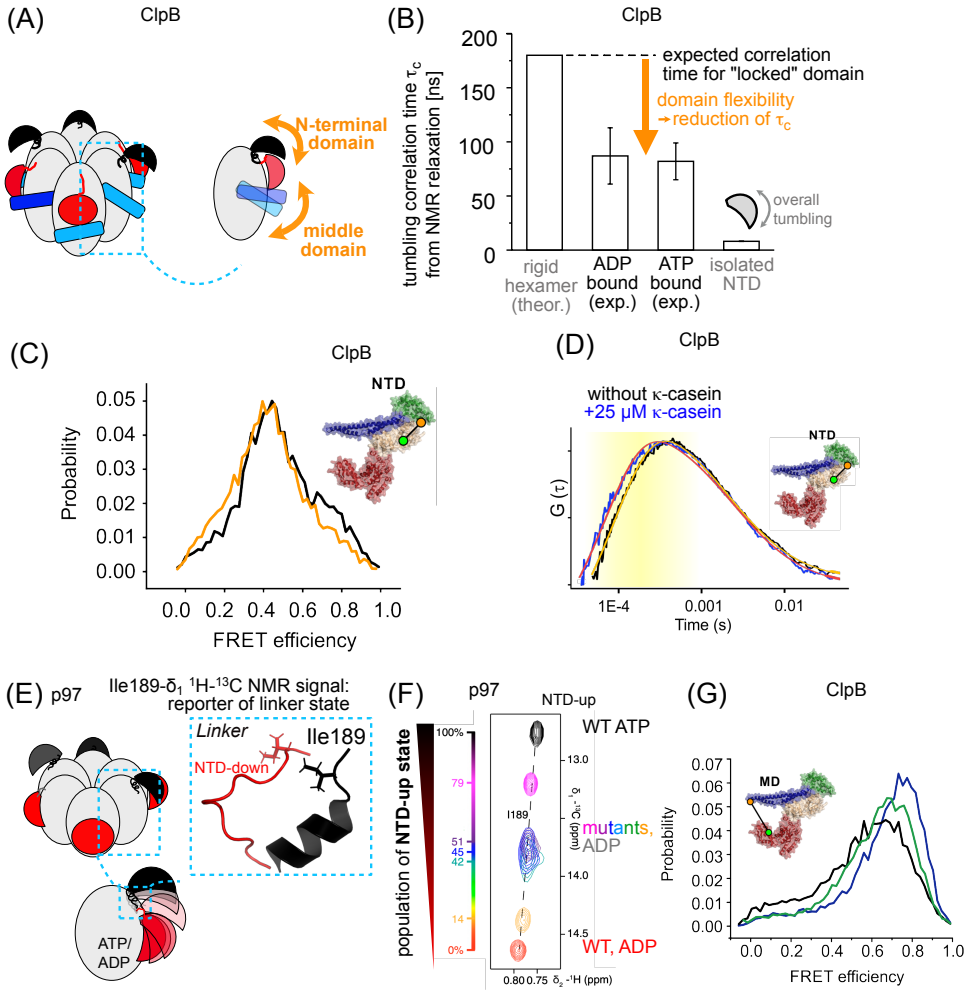

Figure 3: SmFRET and NMR complement each other in studies of AAA+ machine dynamics.

Figure 3: Continued: (A) Schematic view of the structure of the hexameric ClpB disaggregase, highlighting the flexible N-terminal domain (NTD, top) and the middle domain. (B) Tumbling correlation time of the NTD of ClpB determined from methyl relaxation experiments (85). The observed values in both ADP- and ATP-bound states are about 2-fold lower than expected for the case where the NBD was tightly attached (the error margin indicates the span of values reported from different NMR probes within the domain). (C) FRET efficiency histograms measured from a donor-acceptor pair that reports on the motion of the NTD (see inset) with (black) and with (orange) a protein substrate. The broad histograms indicate multiple conformations, with a significant response to the addition of the substrate. (D) Fluorescence cross-correlation curves calculated from single-molecule data without (black) and with the substrate protein (blue). The smooth curves are fits to the data and yield conformational dynamics with a rate of $\sim$10,000 s^{-1}. (E) Schematic view of p97, with a zoom on the linker of the NBD, which harbors a "reporter" residue, Ile189, whose chemical shift differs clearly between the two states. (F) The chemical shift of the δ1 methyl of Ile189 in ATP-bound WT p97 (black; ca. 100% "NTD-up" state), and ADP-bound WT p97 (red, 100% "NTD-down") and ADP-bound mutants which show different levels of NTD-up state. (G) FRET efficiency histograms measured from a donor-acceptor pair that reports on the motion of the MD of ClpB (see inset). The histogram collected from the wild-type protein (black) shifts significantly in a mutant lacking the NTD (green), and even further in the presence of a substrate protein (blue), indicating a transition of the MD to a more active conformation. Panel B was plotted based on data from (85). Panels C,D and G were adapted from (86). Panel F was adapted from (87).

The NTD of ClpB has been suggested to be flexible; indeed, it is frequently not observed in cryo-EM reconstructions (88, 89), though some recent studies did capture partial configurations (90). A truncated NTD version of ClpB was found to exist physiologically in *E. coli* as a mixture with the full length protein (91) and to function similarly to the wild-type, though some studies found the NTD to be essential for cooperative substrate handling and disaggregation regulation (92, 93, 85, 86). The dynamics of the NTD of ClpB have been studied using NMR spectroscopy by Rosenzweig *et al.* (85). To understand how tightly the NBD is attached to the rest of the protein, they determined the rotational correlation time of the NTD from methyl NMR spin relaxation experiments (Fig. 3B); the correlation time is the decay rate constant of the auto-correlation function in Fig. 2L. Rotational correlation times of 87 $\pm$ 26 ns and 82 $\pm$ 17 ns were found in the ADP- and ATP-loaded states found. These values are twice shorter than the overall tumbling time of ClpB, and $\sim$10 times longer than the expected tumbling time of the isolated NTD. This suggests that the NTD has significant domain motion within the hexamer. It does so in both the ATP and ADP bound states, showing that neither of these two states has a "locked" NTD.

Iljina *et al.* labeled the NTD of ClpB with one dye, with a second dye positioned on NBD1 (Fig. 3C), and conducted smFRET experiments on the construct (86). They registered broad FRET efficiency histograms (Fig. 3C), indicative of multiple conformations of the NTD, with a significant shift to lower FRET efficiency values upon protein-substrate binding. The signals were subjected to the photon-by-photon HMM analysis discussed above, and three conformational states were required to obtain an optimal representation of the data, with sub-millisecond dynamics connecting them. FCS also demonstrated microsecond dynamics, with an exchange rate of $\sim$10,000 s^{-1}, which increased in the presence of a substrate protein (Fig. 3D).

While the NMR and smFRET experiments were not designed to observe dynamics on

the same time scale, with the former sensitive to nanosecond tumbling motion and the latter to microsecond-millisecond transitions between semi-stable conformational states, they demonstrated that the NTD utilizes its flexible linker to perform fast motion with respect to the rest of the chaperone. Remarkably, NMR studies of P97/VCP demonstrated similar dynamics of the NTD (94, 87). In particular, a reporter residue, the methyl group of Ile189, has been used as a local probe of the status of the linker region, which indirectly reports on the orientation of the NTD (Fig. 3E). This methyl cross-peak is at distinct positions in the ATP- and ADP-loaded states (Fig. 3F). A CPMG experiment was performed in order to analyze the up-down motion of the NTD, and exchange dynamics with a rate >2,000 s^{-1} were observed, similar to smFRET. Such a fast exchange is expected to average peak positions, i.e. the observed NMR frequency is the population-weighted average of the exchanging conformations (cf. Fig. 2N,O). A shift of the population would lead to a gradual shift of the peak position. Indeed, disease-related mutations in the protein were shown to modulate the equilibrium between the up- and down- conformations of the NTD, as can be read off the chemical shifts in a straightforward manner (Fig. 3F). The domain continued to have some flexibility even in the "up" and "down" states.

As noted above, ClpB also contains the regulatory M-domain as part of its structure, and the lever-like motion of this domain is involved in the regulation of the disaggregation function (39). A curious relation between the dynamics of the NTD and the M-domain was revealed in the study of Iljina *et al.* (86). They showed that the NTD limits the motion of the M-domain, while its removal as well as the binding of a substrate protein allowed the M-domain to attain a more active conformation (Fig. 3G).

3.2. Domain closure in adenylate kinase

The enzyme adenylate kinase (AK) plays a key role in maintaining ATP levels in cells by catalyzing the reaction ATP + AMP $\rightleftharpoons$ ADP + ADP (95, 96). Three domains form the structure of this protein: a large CORE domain into which the smaller LID and nucleotide monophosphate-binding (NMPbind) domains are inserted. The LID domain binds ATP, and the NMPbind domain binds AMP. The major conformational rearrangement of the LID and NMPbind domains upon substrate binding was revealed by X-ray crystallographic studies (97, 98, 99). This movement, termed domain closure, forms the enzyme's active site and excludes solvent molecules from interfering with the chemical reaction, which occurs at a rate of 400 s^{-1}. AK's domain-closure dynamics have been studied using NMR spectroscopy (100, 101, 102, 103), fluorescence experiments, both on the ensemble and single-molecule level (101, 104, 105), and molecular dynamics simulations (106, 107, 108, 109, 110, 111). Based on CPMG NMR experiments, it was suggested that domain opening is rate limiting for the cycle of the protein and determines the relatively slow turnover. Recent smFRET experiments, however, demonstrated that AK's opening and closing rates are significantly faster than suggested based on the NMR studies.

In particular, Aviram *et al.* (113) used experiments with a high photon flux, combined with a photon-by-photon HMM analysis, which allowed them to resolve dynamics on the microsecond time scale (46). In the presence of substrates, domain closure was found to be completed in just a few tens of microseconds, two orders of magnitude faster than turnover. To rationalize this finding, all-atom molecular-dynamics simulations were performed, and a so-called parallel-cascade selection algorithm was used to simulate repeating opening/closing transitions of the enzyme (114). It was found that fast domain movements assist reorienting

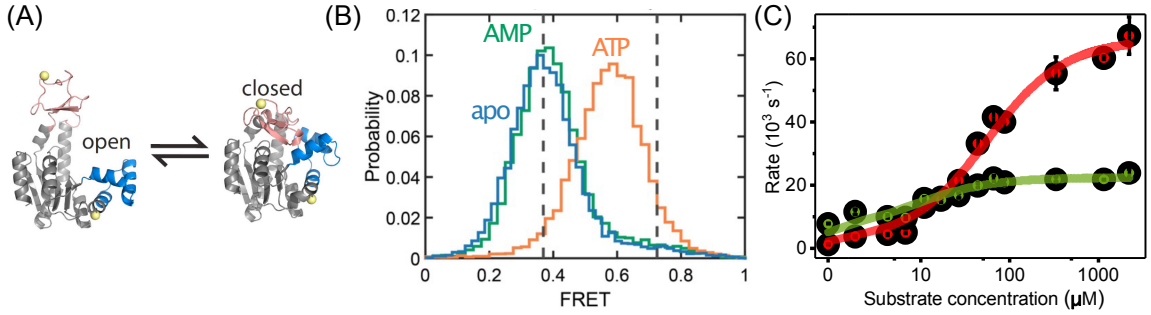

Figure 4: Domain-closure dynamics in adenylate kinase. (A) Schematic structural view of the open and closed conformations. (B) FRET data. In the absence of substrates, the protein is mainly in the open conformation (blue FRET efficiency histogram, open structure depicted on top with the FRET labeling positions in yellow). AMP alone does not lead to a change in the conformational equilibrium (green histogram), but when ATP is added, the histogram shifts to higher FRET efficiency values, indicating a significant population of both open and closed conformations under fast exchange. (C) The rates of interconversion between open and closed conformations increase significantly with substrate concentration. Panels A and B were adapted from (112) and panel C was adapted from (113).

the substrates following incorrect initial binding to the enzyme, allowing them to reach an optimal orientation for catalysis. To shed further light on this question, mutants with different degrees of substrate inhibition by AMP were studied, both biochemically and using smFRET spectroscopy (112). It was shown that inhibitory concentrations of AMP lead to a faster and more cooperative domain closure by ATP, pointing to an allosteric interaction between the domains of AK. A kinetic model that incorporated the rates of domain opening and closing of the substrate-inhibition mutants could explain qualitatively the differences between them. Simulations with the model indicated that the catalytic cycle of AK is affected by the microsecond balance between the open and closed states of the enzyme, rather than by the values of the interconversion rates, as discussed in the second scenario of Figure 1C.

3.3. Functionally important loop motions

The crucial importance of protein dynamics for protein function is particularly well highlighted by the observation that loops are often instrumental for enzyme activity (115, 116, 117, 118, 119, 120, 121, 73, 122). The role of loop dynamics for enzyme function has been treated in several excellent reviews, such as refs. (30, 122).

A case where fast loop motion is important for a catalytic reaction is the aminopeptidase TET2, which assembles to a dodecameric 468 kDa-large tetrahedral particle with a large internal catalytic chamber (123). Crystal structures of TET aminopeptidases showed the vast majority of the protein, but a ca. 20-residue long stretch of the sequence of each protomer was not modeled. These loop structures fill almost 30% of the volume of the catalytic chamber (Fig. 5A). They are "invisible" in the crystal structure, but when removed, the activity is strongly diminished. Gauto *et al.* (121) used MAS NMR to show that the loop undergoes large-amplitude motion, as seen by the order parameters of two reporter residues in the loop (red in Fig. 5B, top): the order parameters are very small only for

these two residues, in line with large amplitude loop motion. Methyl ^{13}C and amide ^{15}N relaxation-dispersion experiments (bottom) allowed to quantify the time scale of this motion, which is tens of μs (at 28 °C). This is much faster than the reaction rate constant (tens of milliseconds), indicating that the kinetics of loop motion do not determine the reaction rate. The authors found that a highly conserved histidine (His) residue in the loop (which is not part of the active site *per se*) is important for stabilising the substrate in the active site (Fig. 5C): functional assays show that mutating the His or shortening the loop leads to a strongly lowered substrate affinity (increased Michaelis constant). Loop dynamics allow this His side chain to reach the substrate in the active site, and its flexibility also allows substrate trafficking in the catalytic chamber. The conformational equilibrium (Fig. 5C) is shifted in the presence of a non-hydrolysable substrate-analog that tightly binds to the active site. This shifting of equilibrium, evidenced by the position of a reporter NMR signal (Val120, Fig. 5D, left), crucially depends on the presence of the His side chain. When this His is replaced by a phenylalanine, the binding of a ligand at the active site does not lead to a conformational redistribution, as evidenced by essentially identical chemical shifts in the apo and holo states (Fig. 5D, right).

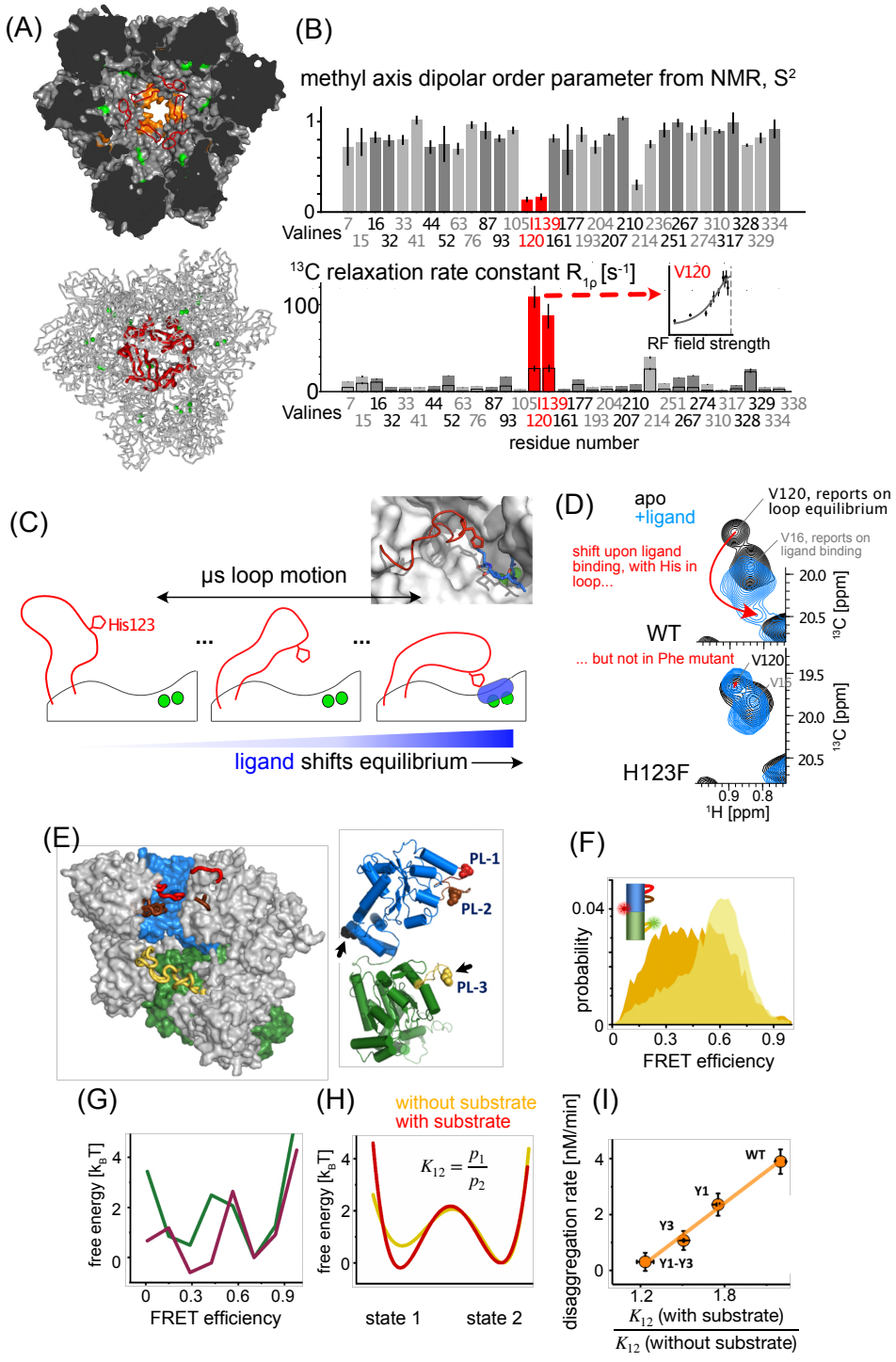

Figure 5

Figure 5: (Preceding page): Functionally important loop motion probed by NMR. (A-D) TET2 aminopeptidase. (A) Structural overview, highlighting the catalytic chamber and the long loop regions (red). (B) NMR dynamics data showing methyl axis order parameters of valines (top), ranging from 1 for rigid sites to 0 for full isotropic motion. The smallest order parameters are obtained in the loop region. The ^{13}C $R_{1\rho}$ relaxation rate constant (bottom) is largest for these residues; together with the observation that $R_{1\rho}$ rates depend on the applied RF field strength (insert), this allows determining the time scale to be tens of µs. (C) Schematic view of loop motion, which can position the conserved His close to the active site (two zinc ions in green). The presence of substrate or inhibitor (blue) shifts the equilibrium towards the right. (D) NMR spectra of WT (left) and H123F mutant without (black) and with (blue) the inhibitor amastatin. (E-I) ClpB. (E) Structure of the ClpB hexamer (left) and protomer (right), indicating the three pore loops in color. (F) FRET efficiency histograms of pore-loop 3 without (yellow) and with (orange) a protein substrate. (G) Analysis of single-molecule data leads to a free-energy landscape for pore-loop 3 without (green) and with (purple) the substrate. (H) This free-energy landscape can be modeled as a two-state profile. (I) A series of mutants demonstrate a linear relation between disaggregation activity and the response of the equilibrium of pore-loop 3 to the substrate. A similar relation was also found for pore-loop 2. Panels A-D were adapted from (121). Panels E-I were adapted from (124).

An additional case of fast loop motion is that of the pore loops of the disaggregation machine already discussed above, ClpB. The pore loops are structural elements protruding into the central channel of the protein, and in ClpB there are three of these, two in NBD1 and one in NBD2 (Fig. 5E) (125). The dynamics of these pore loops have been recently studied with smFRET spectroscopy (124). Each pore loop was labeled in turn, with a second label on a fixed position of the machine (Fig. 5F). FRET efficiency histograms were broad, indicating fast dynamics, and responded to the addition of a substrate protein (Fig. 5F). The motion of the pore loops was indeed found by detailed analysis to be on the sub-millisecond time scale, much faster than disaggregation activity, and their energy landscapes could be modeled in terms of two states, 'up' and 'down' (Fig. 5G-H). Interestingly, a series of mutants demonstrated a linear relation between disaggregation rate and pore-loop conformational responses for two of the pore loops (Fig. 5I), pointing to the importance of pore-loop dynamics for function.

While we emphasize here dynamics that are faster than function, this is not always the case. In several reported studies, the rate of loop motion was similar to the turnover rate. An interesting case that has been well studied by NMR (120), crystallography (126) and simulations(127) is that of protein tyrosine phosphatases.

3.4. When too much of catalytically required motion inhibits function: decapping enzyme

The homodimeric decapping enzyme, DcpS, shows a fascinating link between protein dynamics and function (128). It is formed by an N-terminal β-sheet domain (NTD) and a C-terminal domain (CTD). Formation of the active site requires closure of the NTD onto the CTD. In its apo state, the two protomers of DcpS are symmetric, as evidenced by the fact that a single set of NMR signals is observed. When substrate is added to an amount that results in binding in one of the two active sites, the protein starts exchanging between two states, whereby in each states one of the active sites is in the open conformation and the other in the closed conformation. This exchange, occurring at a rate of about ten per second, is ca. two orders of magnitude faster than the the catalytic rate ($k_{cat} \approx 0.3\text{s}^{-1}$),

suggesting that the rate-limiting step occurs after the formation of the closed state (e.g. rearrangements of the bound substrate). Interestingly, when an excess of the substrate is present, such that both active sites are occupied, the exchange between the states is accelerated (ca. 4-fold). Interestingly, in this situation of fast conformational dynamics, the catalysis is reduced considerably. In other words, the dynamic process, without which catalysis cannot happen, can also inhibit catalysis when it gets too fast, because the time the substrate spends in the closed active site is too short to allow for the chemistry to occur. Interestingly, the authors prepared a mutant protein which, even in excess of substrate, did not accelerate its conformational dynamics the way the WT protein did. This mutant was found to be more active that then WT protein. Overall, this is an interesting case where excess substrate can inhibit activity by inducing excessive dynamics.

3.5. Allosteric regulation in Imidazole glycerol phosphate synthase

Imidazole glycerol phosphate synthase (HisHF) performs two reactions that need to be tightly regulated: one half of the protein (HisH) deaminates glutamine to form glutamate and ammonia, while the other half, the cyclase HisF, uses the ammonia molecule to generate precursors of histidine and purines (129). It is essential that the glutamine hydrolysis is tightly controlled in order not to deplete the glutamine level and produce (toxic) ammonia (130). Indeed, in the absence of the HisF substrate, the HisH activity is very low, but in the presence of a substrate in HisF and a substrate (glutamine) in HisH the deaminase activity is increased by an impressive 4500-fold (131). Wurm *et al.* have used crystallography and solution NMR to demonstrate the basis of this allosteric regulation (132) (Fig. 6). NMR titration experiments with various ligands have revealed that ligand binding is fast (sub-millisecond). The state that has both ligands bound can co-exist in an inactive state and an active state. The exchange between these states occurs on a time scale of ∼100 ms ($k_{I\rightarrow A}$=9 s^{-1},$k_{A\rightarrow I}$=5 s^{-1}), as could be measured by EXSY experiments with a Cys→Ser mutant that undergoes the conformational exchange but is inable to catalyse the reaction (Fig. 6C). Under similar conditions, the catalytic turnover of the WT protein with the same substrate is ca. 0.23 s^{-1}, i.e. 40 times slower than the active-state formation. This finding shows that the catalysis is not determined by the rate constant, but by the population level of the active state (cf. Fig. 1B). To investigate this link further, various mutants, as well as other substrates have been investigated. Indeed, the population of active vs. inactive conformation varies widely between these mutants/ligands, and a strong (although non-linear) correlation between the active-state population and the catalytic turnover rate is observed. Even more so, when the relative destabilisation of the active conformation compared to the wild type is plotted (rather than the absolute population level), a clear linear correlation to the (logarithmic) rate constant is observed (Fig. 6D). This case represents another compelling evidence for fast conformational dynamics underlying slow catalytic turnover, where the population level controls the overall rate constant.

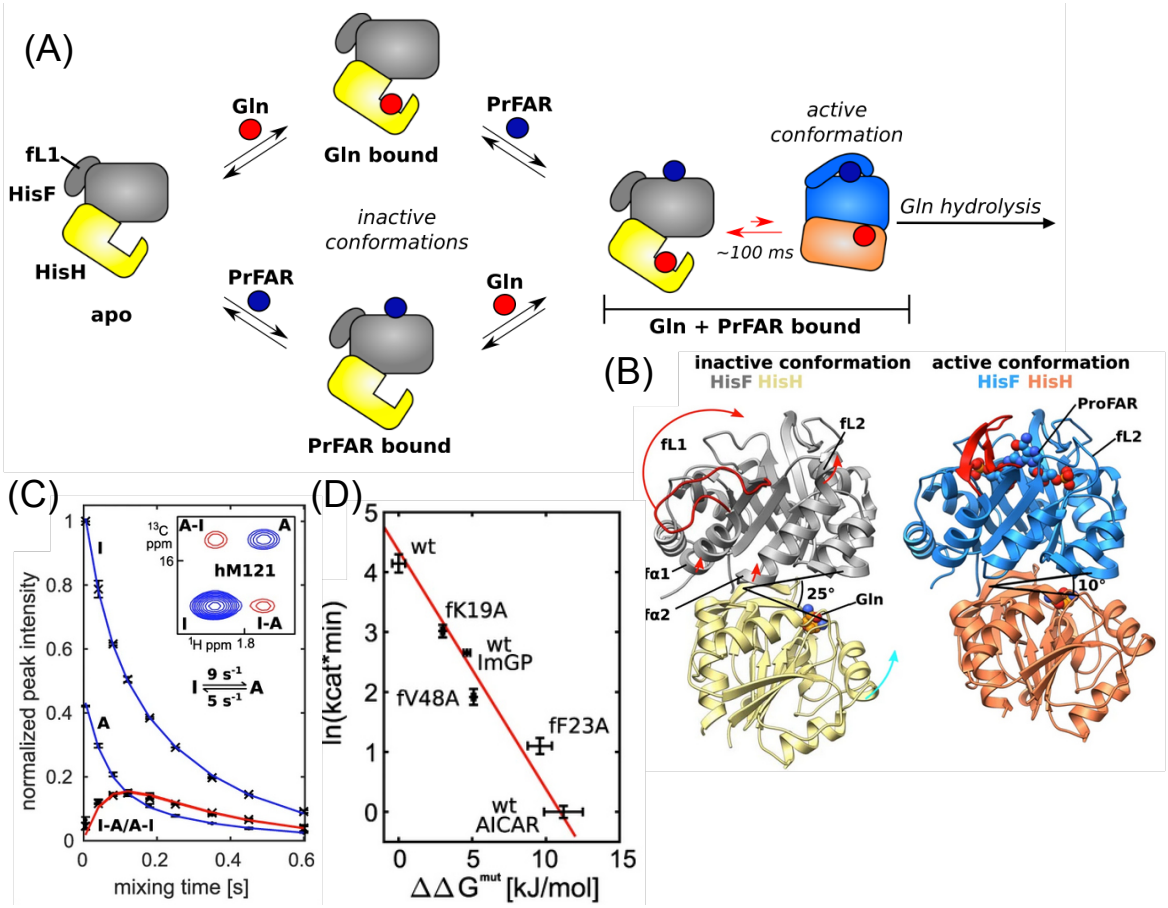

Figure 6: (A) Schematic model of HisHF dynamic function. The two substrates (red, blue) bind to the bienzyme complex rapidly (sub-millisecond). The doubly substrate loaded state (Gln + PrFAR) exchanges slowly ($\sim$ 100 ms) with an active, catalysis competent state (right) to achieve the chemical reaction. (B) Crystal structures of the inactive state (loaded with Gln) and the active state (loaded with both ligands). Important structural changes are indicated in red. (C) EXSY data showing the $\sim$ 100 ms exchange process, here for M121 of HisH. (D) Correlation between the catalytic rate ($\ln(k_{cat})$) of HisFH and $\Delta\Delta G^{mut}$ of the active conformation for different mutants or ligands. Figure adapted from ref. (132).

4. Take-home lessons

In concluding this review, there are two lessons that we would like the readers to take home with them.

First, large-scale conformational dynamics can be essential for the function of proteins, and they often occur on time scales that are much faster than the turnover process. There are various mechanisms, perhaps not all known to us at this point of time, by which fast motions of secondary and tertiary structure elements in proteins couple to the often much-slower functional steps. Using several examples, we have shown here that such fast motions

can control the overall turnover via the equilibrium of states that they establish. In such cases, the equilibrium population of conformational states will affect the protein function. While not our focus here, there might also be cases where motion of a protein element is on a similar time scale to a functional transition, and in this case the kinetics of the conformational dynamics will directly affect function. It is likely that all scenarios in between these two cases exist. The situation becomes even more complex when multiple processes occur simultaneously or when e.g. ligand binding leads to slow rearrangements (133). The link between dynamics and function is, thus, often complex and events on many time scales may be relevant for function, leading to a rich spectrum of behaviors.

Second, deciphering the dynamic activity of a protein is a challenge, because in essence it requires determining 3D structures (already a challenge in itself), and in addition a fourth dimension: time. No single method can tackle this challenge entirely, and several methods should be ideally combined to obtain a more complete picture. SmFRET and NMR methodologies are particularly valuable as experimental techniques for studying conformational fluctuations in functioning proteins. In fact, they complement each other nicely in terms of the typical time- and distance-scales that need to be probed in order to obtain useful information on protein dynamics. We have discussed some cases where smFRET and NMR experiments were harnessed to observe function-related dynamics. As it turns out, there are not (yet) too many examples where both methodologies were applied to the same protein. We hope that in the future such studies will become more common.

Finally, although not discussed in this review, *in silico* methods are extremely valuable in combining the information from different methods and generating a unified picture that can help in the interpretation of experimental results (134). All-atom simulations are still limited in their ability to achieve multi-millisecond simulations that can teach us about the kinetics of large-scale conformational transitions. However, other specialized methods based, e.g., on accelerated molecular dynamics (135), coarse-grained force fields (136) or elastic networks (137) can bridge this gap and have been used to study function-related dynamics and allostery in protein machines. Since the number of works that aim to extend molecular simulations to longer times is quickly increasing (138, 134), we expect that the synergy between computation and experiment will be gradually and significantly enhanced in the coming years.

DISCLOSURE STATEMENT

The authors are not aware of any affiliations, memberships, funding, or financial holdings that might be perceived as affecting the objectivity of this review.

ACKNOWLEDGMENTS

Gilad Haran is the incumbent of the Hilda Pomeraniec Memorial Professorial Chair. He has been partially funded by the European Research Council (ERC) under the European Union's Horizon 2020 research and innovation programme (grant agreement No 742637, SMALLOSTERY), by NSF-BSF grant no. 2021700 and by an ISF Breakthrough grant no. 1924/22. Paul Schanda acknowledges funding from the Austrian Science Fund (FWF; project "AlloSpace", number I05812) and intramural funding from ISTA.

LITERATURE CITED

1. Frauenfelder, H.; Sligar, S. G.; Wolynes, P. G. The energy landscapes and motions of proteins. *Science* **1991**, *254*, 1598–1603.
2. Henzler-Wildman, K.; Kern, D. Dynamic personalities of proteins. *Nature* **2007**, *450*, 964–972.
3. Maity, H.; Muttathukattil, A. N.; Reddy, G. Salt effects on protein folding thermodynamics. *J. Phys. Chem. Lett.* **2018**, *9*, 5063–5070.
4. Lorimer, G. H.; Horovitz, A.; McLeish, T. Allostery and molecular machines. 2018.
5. O'Brien, E. P.; Brooks, B. R.; Thirumalai, D. Effects of pH on proteins: predictions for ensemble and single-molecule pulling experiments. *J. Am. Chem. Soc.* **2012**, *134*, 979–987.
6. Bahar, I.; Jernigan, R. L.; Dill, K. A. *Protein actions: Principles and modeling*; Garland Science, 2017.
7. Wei, G.; Xi, W.; Nussinov, R.; Ma, B. Protein ensembles: how does nature harness thermodynamic fluctuations for life? The diverse functional roles of conformational ensembles in the cell. *Chem. Rev.* **2016**, *116*, 6516–6551.
8. Guo, J.; Zhou, H.-X. Protein allostery and conformational dynamics. *Chem. Rev.* **2016**, *116*, 6503–6515.
9. Haran, G.; Mazal, H. How fast are the motions of tertiary-structure elements in proteins? *J. Chem. Phys.* **2020**, *153*, 130902.
10. Purcell, E. M. Life at Low Reynolds-Number. *Amer. J. Phys.* **1977**, *45*, 3–11.
11. Howard, J. *Mechanics of motor proteins and the cytoskeleton*; Sinauer Associates, 2001.
12. Thirumalai, D.; Hyeon, C.; Zhuravlev, P. I.; Lorimer, G. H. Symmetry, rigidity, and allosteric signaling: from monomeric proteins to molecular machines. *Chem. Rev.* **2019**, *119*, 6788–6821.
13. Khan, Y. A.; White, K. I.; Brunger, A. T. The AAA plus superfamily: a review of the structural and mechanistic principles of these molecular machines. *Crit. Rev. Biochem. Mol. Biol.* **2021**,
14. Grason, J. P.; Gresham, J. S.; Lorimer, G. H. Setting the chaperonin timer: A two-stroke, two-speed, protein machine. *Proc. Natl. Acad. Sci. USA* **2008**, *105*, 17339–17344.
15. Mas, G.; Guan, J.-Y.; Crublet, E.; Debled, E. C.; Moriscot, C.; Gans, P.; Schoehn, G.; Macek, P.; Schanda, P.; Boisbouvier, J. Structural investigation of a chaperonin in action reveals how nucleotide binding regulates the functional cycle. *Sci. Adv.* **2018**, *4*, eaau4196.
16. Lindskog, S. Structure and mechanism of carbonic anhydrase. *Pharmacol Ther* **1997**, *74*, 1–20.
17. Hvidt, A.; Nielsen, S. O. Hydrogen exchange in proteins. *Adv. Prot. Chem.* **1966**, *21*, 287–386.
18. Astumian, R. D.; Hanggi, P. Brownian motors. *Physics Today* **2002**, *55*, 33–39.
19. Haas, E. The study of protein folding and dynamics by determination of intramolecular distance distributions and their fluctuations using ensemble and single-molecule FRET measurements. *ChemPhysChem* **2005**, *6*, 858–870.
20. Alexiev, U.; Farrens, D. L. Fluorescence spectroscopy of rhodopsins: Insights and approaches. *Biochim. Biophys. Acta* **2014**, *1837*, 694–709.
21. Uzawa, T.; Kimura, T.; Ishimori, K.; Morishima, I.; Matsui, T.; Ikeda-Saito, M.; Takahashi, S.; Akiyama, S.; Fujisawa, T. Time-resolved small-angle X-ray scattering investigation of the folding dynamics of heme oxygenase: implication of the scaling relationship for the submillisecond intermediates of protein folding. *J. Mol. Biol.* **2006**, *357*, 997–1008.
22. Callaway, D. J.; Bu, Z. Visualizing the nanoscale: protein internal dynamics and neutron spin echo spectroscopy. *Curr. Opin. Struct. Biol.* **2017**, *42*, 1–5.
23. Ghosh, A.; Ostrander, J. S.; Zanni, M. T. Watching proteins wiggle: Mapping structures with two-dimensional infrared spectroscopy. *Chem. Rev.* **2017**, *117*, 10726–10759.
24. Šrajer, V.; Schmidt, M. Watching proteins function with time-resolved x-ray crystallography. *J. Phys. D Appl. Phys.* **2017**, *50*, 373001.
25. Ando, T.; Uchihashi, T.; Scheuring, S. Filming biomolecular processes by high-speed atomic force microscopy. *Chem. Rev.* **2014**, *114*, 3120–3188.

26. Galazzo, L.; Bordignon, E. Electron Paramagnetic Resonance Spectroscopy in structural-dynamic studies of large protein complexes. *Prog. Nucl. Magn. Reson. Spectrosc.*
27. Torricella, F.; Pierro, A.; Mileo, E.; Belle, V.; Bonucci, A. Nitroxide spin labels and EPR spectroscopy: A powerful association for protein dynamics studies. *Biochim. Biophys. Acta* **2021**, *1869*, 140653.
28. Sekhar, A.; Kay, L. E. An NMR view of protein dynamics in health and disease. *Annu. Rev. Biophys.* **2019**, *48*, 297–319.
29. Anthis, N. J.; Clore, G. M. Visualizing transient dark states by NMR spectroscopy. *Quart. Rev. Biophys.* **2015**, *48*, 35–116.
30. Lisi, G. P.; Loria, J. P. Solution NMR spectroscopy for the study of enzyme allostery. *Chem. Rev.* **2016**, *116*, 6323–6369.
31. Lerner, E.; Barth, A.; Hendrix, J.; Ambrose, B.; Birkedal, V.; Blanchard, S. C.; Börner, R.; Sung Chung, H.; Cordes, T.; Craggs, T. D., et al. FRET-based dynamic structural biology: Challenges, perspectives and an appeal for open-science practices. *eLife* **2021**, *10*, e60416.
32. Forster, T. Zwischenmoleculare Energiewanderung und Fluoreszenz. *Ann. Phys.* **1948**, *2*, 55–75.
33. Stryer, L. Fluorescence energy transfer as a spectroscopic ruler. *Annu. Rev. Biochem.* **1978**, *47*, 819–46.
34. Andrews, D. L.; Demidov, A. A. *Resonance Energy Transfer*; Wiley: Chichester, 1999.
35. Haas, E. The study of protein folding and dynamics by determination of intramolecular distance distributions and their fluctuations using ensemble and single-molecule FRET measurements. *ChemPhysChem* **2005**, *6*, 858–70.
36. Lerner, E. et al. FRET-based dynamic structural biology: Challenges, perspectives and an appeal for open-science practices. *eLife* **2021**, *10*.
37. Mazal, H.; Haran, G. Single-molecule FRET methods to study the dynamics of proteins at work. *Curr. Opin. Biomed. Eng.* **2019**, *12*, 8–17.
38. Brustad, E. M.; Lemke, E. A.; Schultz, P. G.; Deniz, A. A. A general and efficient method for the site-specific dual-labeling of proteins for single molecule fluorescence resonance energy transfer. *J. Am. Chem. Soc.* **2008**, *130*, 17664–5.
39. Mazal, H.; Iljina, M.; Barak, Y.; Elad, N.; Rosenzweig, R.; Goloubinoff, P.; Riven, I.; Haran, G. Tunable Microsecond Dynamics of an Allosteric Switch Regulate the Activity of a AAA+ Disaggregation Machine. *Nat. Commun.* **2019**, *10*, 1438.
40. Roy, R.; Hohng, S.; Ha, T. A practical guide to single-molecule FRET. *Nat. Methods* **2008**, *5*, 507–16.
41. Muller, B. K.; Zaychikov, E.; Brauchle, C.; Lamb, D. C. Pulsed interleaved excitation. *Biophys. J* **2005**, *89*, 3508–22.
42. Torella, J. P.; Holden, S. J.; Santoso, Y.; Hohlbein, J.; Kapanidis, A. N. Identifying molecular dynamics in single-molecule FRET experiments with burst variance analysis. *Biophys. J* **2011**, *100*, 1568–77.
43. Gopich, I. V.; Szabo, A. Single-molecule FRET with diffusion and conformational dynamics. *J. Phys. Chem. B* **2007**, *111*, 12925–12932.
44. Rabiner, L. R. A tutorial on hidden Markov-models and selected applications in speech recognition. *Proc. IEEE* **1989**, *77*, 257–286.
45. Gopich, I. V.; Szabo, A. Decoding the pattern of photon colors in single-molecule FRET. *J. Phys. Chem. B* **2009**, *113*, 10965–73.
46. Pirchi, M.; Tsukanov, R.; Khamis, R.; Tomov, T. E.; Berger, Y.; Khara, D. C.; Volkov, H.; Haran, G.; Nir, E. Photon-by-Photon Hidden Markov Model Analysis for Microsecond Single-Molecule FRET Kinetics. *J. Phys. Chem. B* **2016**, *120*, 13065–13075.
47. Felekyan, S.; Sanabria, H.; Kalinin, S.; Kuhnemuth, R.; Seidel, C. A. Analyzing Forster resonance energy transfer with fluctuation algorithms. *Methods Enzymol* **2013**, *519*, 39–85.
48. Gurunathan, K.; Levitus, M. FRET fluctuation spectroscopy of diffusing biopolymers: contri-

butions of conformational dynamics and translational diffusion. *J. Phys. Chem. B* **2010**, *114*, 980–6.
49. Chowdhury, A.; Nettels, D.; Schuler, B. Interaction Dynamics of Intrinsically Disordered Proteins from Single-Molecule Spectroscopy. *Annu. Rev. Biophys.* **2023**, *52*, 433–462.
50. Cavanagh, J.; Fairbrother, W. J.; Palmer III, A. G.; Skelton, N. J. *Protein NMR spectroscopy: principles and practice*; Academic press, 1996.
51. Zeeb, M.; Balbach, J. Protein folding studied by real-time NMR spectroscopy. *Methods* **2004**, *34*, 65–74.
52. Rennella, E.; Cutuil, T.; Schanda, P.; Ayala, I.; Forge, V.; Brutscher, B. Real-time NMR characterization of structure and dynamics in a transiently populated protein folding intermediate. *J. Am. Chem. Soc.* **2012**, *134*, 8066–8069.
53. Smith, M. J.; Marshall, C. B.; Theillet, F.-X.; Binolfi, A.; Selenko, P.; Ikura, M. Real-time NMR monitoring of biological activities in complex physiological environments. *Curr. Opin. Struct. Biol.* **2015**, *32*, 39–47.
54. Luchinat, E.; Barbieri, L.; Campbell, T. F.; Banci, L. Real-time quantitative in-cell NMR: ligand binding and protein oxidation monitored in human cells using multivariate curve resolution. *Anal. Chem.* **2020**, *92*, 9997–10006.
55. Charlier, C.; Courtney, J. M.; Alderson, T. R.; Anfinrud, P.; Bax, A. Monitoring ^{15}N chemical shifts during protein folding by pressure-jump NMR. *J. Am. Chem. Soc.* **2018**, *140*, 8096–8099.
56. Wand, A. J.; Sharp, K. A. Measuring entropy in molecular recognition by proteins. *Annu. Rev. Biophys.* **2018**, *47*, 41–61.
57. Salvi, N.; Abyzov, A.; Blackledge, M. Atomic resolution conformational dynamics of intrinsically disordered proteins from NMR spin relaxation. *Prog. Nucl. Magn. Reson. Spectrosc.* **2017**, *102*, 43–60.
58. Reif, B.; Ashbrook, S. E.; Emsley, L.; Hong, M. Solid-state NMR spectroscopy. *Nat. Rev. Methods Primers* **2021**, *1*, 2.
59. Schanda, P.; Ernst, M. Studying dynamics by magic-angle spinning solid-state NMR spectroscopy: Principles and applications to biomolecules. *Prog. Nucl. Magn. Reson. Spectrosc.* **2016**, *96*, 1–46.
60. Lamley, J. M.; Öster, C.; Stevens, R. A.; Lewandowski, J. R. Intermolecular Interactions and Protein Dynamics by Solid-State NMR Spectroscopy. *Angew. Chem. Int. Ed.* **2015**, *54*, 15374–15378.
61. Kurauskas, V.; Izmailov, S. A.; Rogacheva, O. N.; Hessel, A.; Ayala, I.; Woodhouse, J.; Shilova, A.; Xue, Y.; Yuwen, T.; Coquelle, N.; Colletier, J.-p.; Skrynnikov, N. R.; Schanda, P. Slow conformational exchange and overall rocking motion in ubiquitin protein crystals. *Nat. Commun.* **2017**, *8*, 145.
62. Krushelnitsky, A.; Gauto, D.; Rodriguez, D. C.; Schanda, P.; Saalwächter, K. Microsecond motions probed by near-rotary-resonance R1ρ 15N MAS NMR experiments : the model case of protein overall-rocking in crystals. *J. Biomol. NMR* **2018**, *71*, 53–67.
63. Good, D.; Pham, C.; Jagas, J.; Lewandowski, R.; Ladizhansky, V. Solid-State NMR Provides Evidence for Small-Amplitude Slow Domain Motions in a Multispanning Transmembrane α -Helical Protein. *J. Am. Chem. Soc.* **2017**, *139*, 9246–9258.
64. Troussicot, L.; Vallet, A.; Molin, M.; Burmann, B. M.; Schanda, P. Disulfide-bond-induced structural frustration and dynamic disorder in a peroxiredoxin from MAS NMR. *J. Am. Chem. Soc.* **2023**, *145*, 10700–10711.
65. Weinhäupl, K.; Lindau, C.; Hessel, A.; Wang, Y.; Schütze, C.; Jores, T.; Melchionda, L.; Schönfisch, B.; Kalbacher, H.; Bersch, B.; Rapaport, D.; Brennich, M.; Lindorff-Larsen, K.; Wiedemann, N.; Schanda, P. Structural Basis of Membrane Protein Chaperoning through the Mitochondrial Intermembrane Space. *Cell* **2018**, *175*, 1365–1379.e25.
66. Burmann, B. M.; Wang, C.; Hiller, S. Conformation and dynamics of the periplasmic

membrane-protein–chaperone complexes OmpX–Skp and tOmpA–Skp. *Nat. Struct. Mol. Biol.* **2013**, *20*, 1265–1272.
67. Vallurupalli, P.; Bouvignies, G.; Kay, L. E. Studying "invisible" excited protein states in slow exchange with a major state conformation. *J. Am. Chem. Soc.* **2012**, *134*, 8148–8161.
68. Bouvignies, G.; Vallurupalli, P.; Hansen, D. F.; Correia, B. E.; Lange, O.; Bah, A.; Vernon, R. M.; Dahlquist, F. W.; Baker, D.; Kay, L. E. Solution structure of a minor and transiently formed state of a T4 lysozyme mutant. *Nature* **2011**, *477*, 111–114.
69. Neudecker, P.; Robustelli, P.; Cavalli, A.; Walsh, P.; Lundstrom, P.; Zarrine-Afsar, A.; Sharpe, S.; Vendruscolo, M.; Kay, L. E. Structure of an Intermediate State in Protein Folding and Aggregation. *Science* **2012**, *336*, 362–366.
70. Orts, J.; Vogeli, B.; Riek, R. Relaxation matrix analysis of spin diffusion for the NMR structure calculation with eNOEs. *J. Chem. Theor. Comput.* **2012**, *8*, 3483–3492.
71. Vögeli, B. The nuclear Overhauser effect from a quantitative perspective. *Prog. NMR Spectrosc.* **2014**, *78*, 1–46.
72. Strotz, D.; Orts, J.; Kadavath, H.; Friedmann, M.; Ghosh, D.; Olsson, S.; Chi, C. N.; Pokharna, A.; Güntert, P.; Vögeli, B., et al. Protein allostery at atomic resolution. *Angew. Chem. Int. Ed.* **2020**, *59*, 22132–22139.
73. Chi, C. N.; Vögeli, B.; Bibow, S.; Strotz, D.; Orts, J.; Güntert, P.; Riek, R. A structural ensemble for the enzyme cyclophilin reveals an orchestrated mode of action at atomic resolution. *Angew. Chem. Int. Ed.* **2015**, *54*, 11657–11661.
74. Vögeli, B.; Orts, J.; Strotz, D.; Chi, C.; Minges, M.; Wälti, M. A.; Güntert, P.; Riek, R. Towards a true protein movie: A perspective on the potential impact of the ensemble-based structure determination using exact NOEs. *J. Magn. Reson.* **2014**, *241*, 53–59.
75. Ashkinadze, D.; Kadavath, H.; Pokharna, A.; Chi, C. N.; Friedmann, M.; Strotz, D.; Kumari, P.; Minges, M.; Cadalbert, R.; Königl, S., et al. Atomic resolution protein allostery from the multi-state structure of a PDZ domain. *Nat. Commun.* **2022**, *13*, 6232.
76. Benitez, J. J.; Keller, A. M.; Ochieng, P.; Yatsunyk, L. A.; Huffman, D. L.; Rosenzweig, A. C.; Chen, P. Probing transient copper Chaperone-Wilson disease protein interactions at the single-molecule level with nanovesicle trapping. *J. Am. Chem. Soc.* **2008**, *130*, 2446–2447.
77. Sanabria, H.; Rodnin, D.; Hemmen, K.; Peulen, T. O.; Felekyan, S.; Fleissner, M. R.; Dimura, M.; Koberling, F.; Kuhnemuth, R.; Hubbell, W.; Gohlke, H.; Seidel, C. A. M. Resolving dynamics and function of transient states in single enzyme molecules. *Nat. Commun.* **2020**, *11*.
78. Vallurupalli, P.; Bouvignies, G.; Kay, L. E. Increasing the exchange time-scale that can be probed by CPMG relaxation dispersion NMR. *J. Phys. Chem. B* **2011**, *115*, 14891–14900.
79. Naudi-Fabra, S.; Tengo, M.; Jensen, M. R.; Blackledge, M.; Milles, S. Quantitative description of intrinsically disordered proteins using single-molecule FRET, NMR, and SAXS. *J. Am. Chem. Soc.* **2021**, *143*, 20109–20121.
80. Naudi-Fabra, S.; Blackledge, M.; Milles, S. Synergies of Single Molecule Fluorescence and NMR for the Study of Intrinsically Disordered Proteins. *Biomolecules* **2022**, *12*, 27.
81. Hanson, P. I.; Whiteheart, S. W. AAA+ proteins: Have engine, will work. *Nat. Rev. Mol. Cell Biol.* **2005**, *6*, 519–529.
82. Lin, J.; Shorter, J.; Lucius, A. L. AAA+ proteins: one motor, multiple ways to work. *Biochem. Soc. Trans.* **2022**, *50*, 895–906.
83. Doyle, S. M.; Genest, O.; Wickner, S. Protein rescue from aggregates by powerful molecular chaperone machines. *Nat. Rev. Mol. Cell Biol.* **2013**, *14*, 617–29.
84. Barthelme, D.; Sauer, R. T. Origin and Functional Evolution of the Cdc48/p97/VCP AAA+ Protein Unfolding and Remodeling Machine. *J. Mol. Biol.* **2016**, *428*, 1861–9.
85. Rosenzweig, R.; Farber, P.; Velyvis, A.; Rennella, E.; Latham, M. P.; Kay, L. E. ClpB N-terminal domain plays a regulatory role in protein disaggregation. *Proc. Natl. Acad. Sci. USA* **2015**, *112*, E6872–81.

86. Iljina, M.; Mazal, H.; Goloubinoff, P.; Riven, I.; Haran, G. Entropic Inhibition: How the Activity of a AAA+ Machine Is Modulated by Its Substrate-Binding Domain. *ACS Chem. Biol.* **2021**, *16*, 775–785.
87. Schutz, A. K.; Rennella, E.; Kay, L. E. Exploiting conformational plasticity in the AAA+ protein VCP/p97 to modify function. *Proc. Natl. Acad. Sci. USA* **2017**, *114*, E6822–E6829.
88. Carroni, M.; Kummer, E.; Oguchi, Y.; Wendler, P.; Clare, D. K.; Sinning, I.; Kopp, J.; Mogk, A.; Bukau, B.; Saibil, H. R. Head-to-tail interactions of the coiled-coil domains regulate ClpB activity and cooperation with Hsp70 in protein disaggregation. *eLife* **2014**, *3*, e02481.
89. Deville, C.; Carroni, M.; Franke, K. B.; Topf, M.; Bukau, B.; Mogk, A.; Saibil, H. R. Structural pathway of regulated substrate transfer and threading through an Hsp100 disaggregase. *Sci. Adv.* **2017**, *3*, e1701726.
90. Rizo, A. N.; Lin, J.; Gates, S. N.; Tse, E.; Bart, S. M.; Castellano, L. M.; DiMaio, F.; Shorter, J.; Southworth, D. R. Structural basis for substrate gripping and translocation by the ClpB AAA+ disaggregase. *Nat. Commun.* **2019**, *10*, 2393.
91. Squires, C. L.; Pedersen, S.; Ross, B. M.; Squires, C. ClpB is the Escherichia coli heat shock protein F84.1. *J. Bacteriol* **1991**, *173*, 4254–62.
92. Mizuno, S.; Nakazaki, Y.; Yoshida, M.; Watanabe, Y. H. Orientation of the amino-terminal domain of ClpB affects the disaggregation of the protein. *FEBS J.* **2012**, *279*, 1474–84.
93. Sweeny, E. A.; Jackrel, M. E.; Go, M. S.; Sochor, M. A.; Razzo, B. M.; DeSantis, M. E.; Gupta, K.; Shorter, J. The Hsp104 N-terminal domain enables disaggregase plasticity and potentiation. *Mol. Cell* **2015**, *57*, 836–849.
94. Schuetz, A. K.; Kay, L. E. A Dynamic molecular basis for malfunction in disease mutants of p97/VCP. *eLife* **2016**, *5*.
95. Noma, T. Dynamics of nucleotide metabolism as a supporter of life phenomena. *J. Med. Invest.* **2005**, *52*, 127–136.
96. Dzeja, P.; Terzic, A. Adenylate kinase and AMP signaling networks: metabolic monitoring, signal communication and body energy sensing. *Int. J. Mol. Sci.* **2009**, *10*, 1729–1772.
97. Schulz, G. E.; Müller, C. W.; Diederichs, K. Induced-fit movements in adenylate kinases. *J. Mol. Biol.* **1990**, *213*, 627–630.
98. Müller, C. W.; Schulz, G. E. Structure of the complex between adenylate kinase from Escherichia coli and the inhibitor Ap5A refined at 1.9 Å resolution: A model for a catalytic transition state. *J. Mol. Biol.* **1992**, *224*, 159–177.
99. Vonrhein, C.; Schlauderer, G. J.; Schulz, G. E. Movie of the structural changes during a catalytic cycle of nucleoside monophosphate kinases. *Structure* **1995**, *3*, 483–490.
100. Wolf-Watz, M.; Thai, V.; Henzler-Wildman, K.; Hadjipavlou, G.; Eisenmesser, E. Z.; Kern, D. Linkage between dynamics and catalysis in a thermophilic-mesophilic enzyme pair. *Nat. Struct. Mol. Biol.* **2004**, *11*, 945–949.
101. Henzler-Wildman, K. A.; Thai, V.; Lei, M.; Ott, M.; Wolf-Watz, M.; Fenn, T.; Pozharski, E.; Wilson, M. A.; Petsko, G. A.; Karplus, M.; Kern, D. Intrinsic motions along an enzymatic reaction trajectory. *Nature* **2007**, *450*, 838–844.
102. Kovermann, M.; Ådén, J.; Grundström, C.; Sauer-Eriksson, A. E.; Sauer, U. H.; Wolf-Watz, M. Structural basis for catalytically restrictive dynamics of a high-energy enzyme state. *Nat. Commun.* **2015**, *6*, 7644–7644.
103. Schrank, T. P.; Bolen, D. W.; Hilser, V. J. Rational modulation of conformational fluctuations in adenylate kinase reveals a local unfolding mechanism for allostery and functional adaptation in proteins. *Proc. Natl. Acad. Sci. USA* **2009**, *106*, 16984–16989.
104. Sinev, M. A.; Sineva, E. V.; Ittah, V.; Haas, E. Domain Closure in Adenylate Kinase. *Biochemistry* **1996**, *35*, 6425–6437.
105. Hanson, J. A.; Duderstadt, K.; Watkins, L. P.; Bhattacharyya, S.; Brokaw, J.; Chu, J.-W.; Yang, H. Illuminating the mechanistic roles of enzyme conformational dynamics. *Proc. Natl. Acad. Sci. USA* **2007**, *104*, 18055–18060.

106. Lee, J.; Joo, K.; Brooks, B. R.; Lee, J. The atomistic mechanism of conformational transition of adenylate kinase investigated by Lorentzian structure-based potential. *J. Chem. Theory. Comput.* **2015**, *11*, 3211–3224.
107. Li, W.; Wang, J.; Zhang, J.; Takada, S.; Wang, W. Overcoming the Bottleneck of the Enzymatic Cycle by Steric Frustration. *Phys. Rev. Lett.* **2019**, *122*, 238102.
108. Zheng, Y.; Cui, Q. Multiple Pathways and Time Scales for Conformational Transitions in apo-Adenylate Kinase. *J. Chem. Theor. Comput.* **2018**, *14*, 1716–1726.
109. Whitford, P. C.; Miyashita, O.; Levy, Y.; Onuchic, J. N. Conformational Transitions of Adenylate Kinase: Switching by Cracking. *J. Mol. Biol.* **2007**, *366*, 1661–1671.
110. Formoso, E.; Limongelli, V.; Parrinello, M. Energetics and Structural Characterization of the large-scale Functional Motion of Adenylate Kinase. *Sci. Rep.* **2015**, *5*, 8425.
111. Maragakis, P.; Karplus, M. Large Amplitude Conformational Change in Proteins Explored with a Plastic Network Model: Adenylate Kinase. *J. Mol. Biol.* **2005**, *352*, 807–822.
112. Scheerer, D.; Adkar, B. V.; Bhattacharyya, S.; Levy, D.; Iljina, M.; Riven, I.; Dym, O.; Haran, G.; Shakhnovich, E. I. Allosteric communication between ligand binding domains modulates substrate inhibition in adenylate kinase. *Proc. Natl. Acad. Sci. USA* **2023**, *120*, e2219855120.
113. Aviram, H. Y.; Pirchi, M.; Mazal, H.; Barak, Y.; Riven, I.; Haran, G. Direct observation of ultrafast large-scale dynamics of an enzyme under turnover conditions. *Proc. Natl. Acad. Sci. USA* **2018**, *115*, 3243–3248.
114. Lu, J.; Scheerer, D.; Wang, W.; Haran, G.; Li, W. Role of repeated conformational transitions in substrate binding of adenylate kinase. *J. Phys. Chem. B* **2022**, *126*, 8188–9201.
115. Gerstein, M.; Chothia, C. Analysis of protein loop closure: two types of hinges produce one motion in lactate dehydrogenase. *J. Mol. Biol* **1991**, *220*, 133–149.
116. Whittier, S. K.; Hengge, A. C.; Loria, J. P. Conformational motions regulate phosphoryl transfer in related protein tyrosine phosphatases. *Science* **2013**, *341*, 899–903.
117. Fetrow, J. S. Omega loops; nonregular secondary structures significant in protein function and stability. *FASEB J.* **1995**, *9*, 708–717.
118. Rozovsky, S.; Jogl, G.; Tong, L.; McDermott, A. E. Solution-state NMR investigations of triosephosphate isomerase active site loop motion: ligand release in relation to active site loop dynamics. *J. Mol. Biol.* **2001**, *310*, 271–280.
119. Johnson, T. A.; Holyoak, T. Increasing the conformational entropy of the Ω-loop lid domain in phosphoenolpyruvate carboxykinase impairs catalysis and decreases catalytic fidelity. *Biochemistry* **2010**, *49*, 5176–5187.
120. Cui, D. S.; Lipchock, J. M.; Brookner, D.; Loria, J. P. Uncovering the molecular interactions in the catalytic loop that modulate the conformational dynamics in protein tyrosine phosphatase 1B. *J. Am. Chem. Soc.* **2019**, *141*, 12634–12647.
121. Gauto, D. F.; Macek, P.; Malinverni, D.; Fraga, H.; Paloni, M.; Sučec, I.; Hessel, A.; Bustamante, J. P.; Barducci, A.; Schanda, P. Functional control of a 0.5 MDa TET aminopeptidase by a flexible loop revealed by MAS NMR. *Nat. Commun.* **2022**, *13*, 1927.
122. Corbella, M.; Pinto, G. P.; Kamerlin, S. C. Loop dynamics and the evolution of enzyme activity. *Nat. Rev. Chem.* **2023**, 1–12.
123. Appolaire, A.; Colombo, M.; Basbous, H.; Gabel, F.; Girard, E.; Franzetti, B. TET peptidases: A family of tetrahedral complexes conserved in prokaryotes. *Biochimie* **2016**, *122*, 188–196.
124. Mazal, H.; Iljina, M.; Riven, I.; Haran, G. Ultrafast pore-loop dynamics in a AAA+ machine point to a Brownian-ratchet mechanism for protein translocation. *Sci. Adv.* **2021**, *7*, eabg4674.
125. Lee, J.; Sung, N.; Yeo, L.; Chang, C.; Lee, S.; Tsai, F. T. F. Structural determinants for protein unfolding and translocation by the Hsp104 protein disaggregase. *Biosci. Rep.* **2017**, *37*.
126. Keedy, D. A.; Hill, Z. B.; Biel, J. T.; Kang, E.; Rettenmaier, T. J.; Brandao-Neto, J.; Pearce, N. M.; von Delft, F.; Wells, J. A.; Fraser, J. S. An expanded allosteric network in

PTP1B by multitemperature crystallography, fragment screening, and covalent tethering. *eLife* **2018**, *7*, e36307.
127. Crean, R. M.; Biler, M.; van der Kamp, M. W.; Hengge, A. C.; Kamerlin, S. C. Loop dynamics and enzyme catalysis in protein tyrosine phosphatases. *J. Am. Chem. Soc.* **2021**, *143*, 3830–3845.
128. Neu, A.; Neu, U.; Fuchs, A.-L.; Schlager, B.; Sprangers, R. An excess of catalytically required motions inhibits the scavenger decapping enzyme. *Nat. Chem. Biol.* **2015**, *11*, 697–704.
129. Mouilleron, S.; Golinelli-Pimpaneau, B. Conformational changes in ammonia-channeling glutamine amidotransferases. *Curr. Opin. Struct. Biol.* **2007**, *17*, 653–664.
130. List, F.; Vega, M. C.; Razeto, A.; Häger, M. C.; Sterner, R.; Wilmanns, M. Catalysis uncoupling in a glutamine amidotransferase bienzyme by unblocking the glutaminase active site. *Chem. Biol.* **2012**, *19*, 1589–1599.
131. Beismann-Driemeyer, S.; Sterner, R. Imidazole Glycerol Phosphate Synthase fromThermotoga maritima: quarternary structure, steady-state kinetics and reaction mechanism of the bienzyme complex. *J. Biol. Chem.* **2001**, *276*, 20387–20396.
132. Wurm, J. P.; Sung, S.; Kneuttinger, A. C.; Hupfeld, E.; Sterner, R.; Wilmanns, M.; Sprangers, R. Molecular basis for the allosteric activation mechanism of the heterodimeric imidazole glycerol phosphate synthase complex. *Nat. Commun.* **2021**, *12*, 2748.
133. Ainslie Jr, G. R.; Shill, J. P.; Neet, K. E. Transients and cooperativity: a slow transition model for relating transients and cooperative kinetics of enzymes. *J. Biol. Chem.* **1972**, *247*, 7088–7096.
134. Bottaro, S.; Lindorff-Larsen, K. Biophysical experiments and biomolecular simulations: A perfect match? *Science* **2018**, *361*, 355–360.
135. Markwick, P. R. L.; McCammon, J. A. Studying functional dynamics in bio-molecules using accelerated molecular dynamics. *Phys. Chem. Chem. Phys.* **2011**, *13*, 20053–20065.
136. Hyeon, C.; Thirumalai, D. Capturing the essence of folding and functions of biomolecules using coarse-grained models. *Nat. Commun.* **2011**, *2*, 487.
137. Bahar, I.; Lezon, T. R.; Yang, L. W.; Eyal, E. Global dynamics of proteins: bridging between structure and function. *Annu. Rev. Biophys.* **2010**, *39*, 23–42.
138. Chen, H.; Chipot, C. Enhancing sampling with free-energy calculations. *Curr. Opin. Struct. Biol.* **2022**, *77*, 102497.